



Projected land ice contributions to twenty-first-century sea level rise

Tamsin L. Edwards, Sophie M.J. Nowicki, Ben Marzeion, Regine Hock, Heiko Goelzer, Hélène Seroussi, Nicolas Jourdain, Donald A. Slater, Fiona E. Turner, Christopher J. Smith, et al.

► To cite this version:

Tamsin L. Edwards, Sophie M.J. Nowicki, Ben Marzeion, Regine Hock, Heiko Goelzer, et al.. Projected land ice contributions to twenty-first-century sea level rise. *Nature*, 2021, 593 (7857), pp.74-82. 10.1038/s41586-021-03302-y . hal-03230877

HAL Id: hal-03230877

<https://hal.science/hal-03230877>

Submitted on 16 Sep 2021

HAL is a multi-disciplinary open access archive for the deposit and dissemination of scientific research documents, whether they are published or not. The documents may come from teaching and research institutions in France or abroad, or from public or private research centers.

L'archive ouverte pluridisciplinaire **HAL**, est destinée au dépôt et à la diffusion de documents scientifiques de niveau recherche, publiés ou non, émanant des établissements d'enseignement et de recherche français ou étrangers, des laboratoires publics ou privés.

ARTICLE

Projected land ice contributions to 21st century sea level rise

Tamsin L. Edwards^{1*}, Sophie Nowicki^{2,58}, Ben Marzeion^{6,7}, Regine Hock^{14,52}, Heiko Goelzer^{3,4,53}, Hélène Seroussi⁵, Nicolas C. Jourdain⁹, Donald Slater^{10,51}, Fiona Turner¹, Christopher J. Smith⁸, Christine M. McKenna⁸, Erika Simon², Ayako Abe-Ouchi¹¹, Jonathan M. Gregory^{12,13}, Eric Larour⁵, William H. Lipscomb¹⁵, Antony J. Payne¹⁶, Andrew Shepherd¹⁷, Cécile Agosta¹⁸, Patrick Alexander^{19,20}, Torsten Albrecht²¹, Brian Anderson²², Xylar Asay-Davis²³, Andy Aschwanden¹⁴, Alice Barthel²³, Andrew Bliss²⁴, Reinhard Calov²¹, Christopher Chambers²⁵, Nicolas Champollion^{6,9}, Youngmin Choi^{26,5}, Richard Cullather², Joshua Cuzzone⁵, Christophe Dumas¹⁸, Denis Felikson^{2,57}, Xavier Fettweis²⁸, Koji Fujita²⁹, Benjamin K. Galton-Fenzi^{27,44}, Rupert Gladstone⁴⁷, Nicholas R. Golledge²², Ralf Greve^{25,56}, Tore Hattermann^{30,31}, Matthew J. Hoffman²³, Angelika Humbert^{32,48}, Matthias Huss^{33,34,35}, Philippe Huybrechts³⁶, Walter Immerzeel³⁷, Thomas Kleiner³², Philip Kraaijenbrink³⁷, Sébastien Lecocq³⁶, Victoria Lee³⁸, Gunter R. Leguy¹⁵, Christopher M. Little³⁹, Daniel P. Lowry⁴⁹, Jan-Hendrik Malles^{6,7}, Daniel F. Martin⁵⁰, Fabien Maussion⁴⁰, Mathieu Morlighem²⁶, James F. O'Neill¹, Isabel Nias^{2,55}, Frank Pattyn⁴, Tyler Pelle²⁶, Stephen Price²³, Aurélien Quiquet¹⁸, Valentina Radić⁴¹, Ronja Reese²¹, David R. Rounce¹⁴, Martin Rückamp³², Akiko Sakai²⁹, Courtney Shafer⁵⁰, Nicole-Jeanne Schlegel⁵, Sarah Shannon¹⁶, Robin S. Smith¹², Fiammetta Straneo¹⁰, Sainan Sun⁴, Lev Tarasov⁴², Luke D. Trusel⁴³, Jonas Van Breedam³⁶, Roderik van de Wal^{3,37}, Michiel van den Broeke³, Ricarda Winkelmann^{21,54}, Harry Zekollari^{45,4,33,34}, Chen Zhao⁴⁴, Tong Zhang²³, Thomas Zwinger⁴⁶

* Corresponding author

1 Department of Geography, King's College London, London, UK

2 NASA Goddard Space Flight Center, Greenbelt, MD, USA

3 Institute for Marine and Atmospheric research Utrecht, Utrecht University, The Netherlands

4 Laboratoire de Glaciologie, Université Libre de Bruxelles, Brussels, Belgium

5 Jet Propulsion Laboratory, California Institute of Technology, Pasadena, CA, USA

32 6 Institute of Geography, University of Bremen, Germany
 33 7 MARUM – Center for Marine Environmental Sciences, University of Bremen, Germany
 34 8 Priestley International Centre for Climate, University of Leeds, Leeds, UK
 35 9 Univ. Grenoble Alpes/CNRS/IRD/G-INP, Institut des Géosciences de l'Environnement, France
 36 10 Scripps Institution of Oceanography, University of California San Diego, La Jolla, CA, USA
 37 11 Atmosphere and Ocean Research Institute, The University of Tokyo, Kashiwa-shi, Chiba 277-8564,
 38 Japan
 39 12 National Centre for Atmospheric Science, University of Reading, Reading, UK
 40 13 Met Office, Hadley Centre, Exeter, UK
 41 14 Department of Civil and Environmental Engineering, Carnegie Mellon University, USA
 42 15 Climate and Global Dynamics Laboratory, National Center for Atmospheric Research, Boulder, CO,
 43 USA
 44 16 School of Geographical Sciences, University of Bristol, Bristol, UK
 45 17 Centre for Polar Observation and Modelling, School of Earth and Environment, University of Leeds,
 46 Leeds, LS2 9JT, UK
 47 18 Laboratoire des sciences du climat et de l'environnement, LSCE-IPSL, CEA-CNRS-UVSQ, Université
 48 Paris-Saclay, France
 49 19 Lamont-Doherty Earth Observatory, Columbia University, Palisades, NY, USA
 50 20 NASA Goddard Institute for Space Studies, New York, NY, USA
 51 21 Potsdam Institute for Climate Impact Research (PIK), Member of the Leibniz Association, Potsdam,
 52 Germany
 53 22 Antarctic Research Centre, Victoria University of Wellington, New Zealand
 54 23 Theoretical Division, Los Alamos National Laboratory, Los Alamos, NM, USA
 55 24 Department of Anthropology and Geography, Colorado State University, USA
 56 25 Institute of Low Temperature Science, Hokkaido University, Sapporo, Japan
 57 26 Department of Earth System Science, University of California Irvine, Irvine, CA, USA
 58 27 Australian Antarctic Division, Kingston, Tasmania, Australia
 59 28 Laboratory of Climatology, Department of Geography, University of Liège, Liège, Belgium
 60 29 Graduate School of Environmental Studies, Nagoya University, Nagoya, Japan
 61 30 Norwegian Polar Institute, Tromsø, Norway
 62 31 Energy and Climate Group, Department of Physics and Technology, The Arctic University – University
 63 of Tromsø, Tromsø, Norway
 64 32 Alfred-Wegener-Institut Helmholtz-Zentrum für Polar- und Meeresforschung, Bremerhaven, Germany
 65 33 Laboratory of Hydraulics, Hydrology and Glaciology (VAW), ETH Zurich, Switzerland
 66 34 Swiss Federal Institute for Forest, Snow and Landscape Research (WSL), Birmensdorf, Switzerland
 67 35 Department of Geosciences, University of Fribourg, Switzerland
 68 36 Earth System Science and Departement Geografie, Vrije Universiteit Brussel, Brussels, Belgium
 69 37 Department of Physical Geography, Utrecht University, The Netherlands

38 Centre for Polar Observation and Modelling, School of Geographical Sciences, University of Bristol,
 Bristol, UK

39 Atmospheric and Environmental Research, Inc., Lexington, Massachusetts, USA

40 Department of Atmospheric and Cryospheric Sciences, University of Innsbruck, Austria

41 Department of Earth, Ocean and Atmospheric Sciences, University of British Columbia, Canada

42 Dept of Physics and Physical Oceanography, Memorial University of Newfoundland, Canada

43 Department of Geography, Pennsylvania State University, University Park, PA, USA

44 Australian Antarctic Program Partnership, Institute for Marine and Antarctic Studies, University of
 Tasmania, Hobart, Tasmania

45 Department of Geoscience and Remote Sensing, Delft University of Technology, The Netherlands

46 CSC-IT Center for Science, Espoo, Finland

47 Arctic Centre, University of Lapland, Finland

48 Department of Geoscience, University of Bremen, Bremen, Germany

49 GNS Science, Lower Hutt, New Zealand

50 Computational Research Division, Lawrence Berkeley National Laboratory, Berkeley, CA, USA

51 School of Geography and Sustainable Development, University of St Andrews, UK

52 Department of Geosciences, University of Oslo, Norway

53 NORCE Norwegian Research Centre, Bjerknes Centre for Climate Research, Bergen, Norway

54 Department of Physics and Astronomy, University of Potsdam, Potsdam, Germany

55 School of Environmental Sciences, University of Liverpool, Liverpool, UK

56 Arctic Research Center, Hokkaido University, Sapporo, Japan

57 Universities Space Research Association, Goddard Earth Sciences Technology and Research Studies
 and Investigations, Columbia, MD 21044, USA

58 Geology Department and RENEW Institute, University at Buffalo, Buffalo, NY, USA

**The land ice contribution to global mean sea level rise has not yet been predicted¹ with
 ice sheet and glacier models for the latest set of socio-economic scenarios, nor with
 coordinated exploration of uncertainties arising from the various computer models
 involved. Two recent international projects generated a large suite of projections using
 multiple models^{2-3,5,8,14-16}, but mostly used previous generation scenarios⁹ and climate
 models²¹, and could not fully explore known uncertainties. Here we estimate probability
 distributions for these projections under the new scenarios^{19,30} using statistical
 emulation of the ice sheet and glacier models, and find that limiting global warming to
 1.5°C would halve the land ice contribution to 21st century sea level rise, relative to
 current emissions pledges. The median decreases from 25 to 13 cm sea level equivalent
 (SLE) by 2100, with glaciers responsible for half the sea level contribution. The
 Antarctic contribution does not show a clear response to emissions scenario, due to**

competing processes of increasing ice loss and snowfall accumulation in a warming climate. However, under risk-averse (pessimistic) assumptions, Antarctic ice loss could be five times higher, increasing the median land ice contribution to 42 cm SLE under current policies and pledges, with the upper end (95th percentile) exceeding half a metre even under 1.5°C warming. This would severely limit the possibility of mitigating future coastal flooding. Given this large range (13 cm main projections under 1.5°C warming; 42 cm risk-averse projections under current pledges), adaptation must plan for a factor of three uncertainty in the land ice contribution to 21st century sea level rise until climate policies and the Antarctic response are further constrained.

Land ice has contributed around half of all sea level rise since 1993, and this fraction is expected to increase¹. The Ice Sheet Model Intercomparison Project (ISMIP6^{2,3}) for CMIP6⁴ and the Glacier Model Intercomparison Project (GlacierMIP⁵) provide the Intergovernmental Panel on Climate Change (IPCC) with projections of Earth's ice sheet and glacier contributions to future sea level. Both projects use suites of numerical models^{6,7,8} and greenhouse gas emission scenarios⁹ as the basis of their projections, and a variety of treatments are considered for the interaction between the ice sheets and the ocean^{10,11,12,13}. In total, the projects provide 256 simulations of the Greenland ice sheet, 344 simulations of the Antarctic ice sheet, and 288 simulations of the global glacier response to climate change^{8,14,15,16} (see also Extended Data Table 1). Although these simulations represent an unprecedented effort^{3,6,7,8,10-18}, their computational expense and complexity has meant that they (i) focus mainly on previous generation emissions scenarios (Representation Concentration Pathways⁹, RCPs) developed for the IPCC's Fifth Assessment Report, not the more diverse and policy-relevant Shared Socioeconomic Pathways (SSPs^{19,20}) that underpin the IPCC's Sixth Assessment Report, (ii) are driven mostly by a relatively small number of older generation global climate models developed before CMIP6²¹, and (iii) have incomplete and limited ensemble designs.

To address these limitations, we emulate the future sea level contribution of the 23 regions comprising the world's land ice (see Extended Data Table 2) as a function of global mean surface air temperature change and as a consequence of marine-terminating glacier retreat in Greenland and ice-shelf basal melting and collapse in Antarctica. The ensembles of ice sheet and glacier models are emulated all at once for each region, using their simulations as

multiple estimates of sea level contribution for a given set of uncertain input values, and we incorporate the ensemble spread through the use of a ‘nugget’ term in Gaussian Process emulation^{22,23}. Gaussian Process regression requires minimal assumptions about the functional form, and provides uncertainty estimates for the emulator predictions²⁴; most previous emulator-type approaches for sea level rise use parametric models, where the functional form is assumed²⁵⁻²⁹. We then use the emulators to make probabilistic projections for the glacier and ice sheet sea level contributions under five SSPs and under an additional scenario reflecting current climate pledges (Nationally Determined Contributions, NDCs)³⁰ made under the Paris Agreement. Most projections presented are for the year 2100, but we also estimate a full timeseries by emulating each year from 2016 to 2100. The details of our emulation approach are described in the Methods.

Response to temperature and parameters

Most land ice regions show a fairly linear relationship of increasing mass loss with global mean surface air temperature. Figure 1 shows the temperature-dependence of the sea level contribution at 2100 for the ice sheets and peripheral glaciers (Fig. 1 a-f) and eleven other glacier regions: four with large maximum contributions (Alaska, Arctic Canada North and South, Russian Arctic: Fig. 1g-j), two with non-linear temperature-dependence, giving near or total disappearance at high temperatures (Central Europe and Caucasus: Fig. 1k, l), and the three regions comprising High Mountain Asia (Fig. 1m-o), which are important for local water supply³². Values of ice sheet parameters are fixed at two possible values for Greenland glacier retreat and Antarctic basal melting, with no Antarctic ice shelf collapse; only simulations using these values are shown. The ensemble designs are not complete – for example, many fewer ice sheet simulations were performed under RCP2.6 than RCP8.5 – so some of the apparent patterns in the simulation data are artefacts of the gaps, which the emulator is intended to account for.

Greenland and the glaciers, which are dominated by surface melting^{8,14,16}, show clear dependence on temperature. Fourteen of the nineteen glacier regions show approximately linear relationships, and five are nonlinear (Fig. 1f, k, l; also Western Canada & U.S. and North Asia, which have weaker nonlinearity: not shown). In contrast, East Antarctica (Fig. 1c) shows a slight decrease in sea level contribution with temperature: snowfall increases,

because warmer air can hold more water vapour, and this dominates over the increase in mass loss due to melting^{15,16}. Finally, West Antarctica and the Peninsula (b, e) show little detectable temperature-dependence, due to an approximate cancellation across varying climate and ice sheet model predictions of snowfall accumulation and ice loss. Antarctic ice sheet results are discussed in detail later (see 'Antarctic focus').

The ice sheet contributions depend strongly on the Greenland glacier retreat and Antarctic sub-shelf basal melting parameters, which determine the sensitivity of the marine-terminating glaciers to ocean temperatures (and surface meltwater runoff for Greenland). Figure 2 shows these relationships; the Greenland parameter is defined such that more negative values correspond to further retreat inland.

Land ice contributions in 2100

We use probability distributions for global mean surface air temperature (Fig. 3a: FaIR simple climate model³⁰) and ice-ocean parameters (Figs. 3b and 3c show κ and γ , which are derived from the original parameterisation studies; ice shelf collapse is assigned equal probability off/on) as inputs to the emulators. Time series projections for the land ice contribution under all scenarios are shown in Fig. 3d, and probability density functions at 2100 for the Greenland ice sheet, Arctic Canada North, the glacier total, and West and East Antarctica in Fig. 3e-i. The Antarctic ice sheet total under the NDCs is shown in (j). ('Risk-averse' projections in (d) and (j) are discussed later.) Density estimates are less smooth for the glacier and Antarctica totals than individual regions, because sums of regions are estimated by random sampling rather than deterministic integration; these samples are shown for Antarctica (j).

Our projections show that reducing greenhouse gas emissions from current and projected pledges under the Paris Agreement (NDCs) enough to limit warming to 1.5 °C (SSP1-19) would nearly halve the land ice contribution to sea level at 2100 (Table 1: median decreases from 25 cm to 14 cm SLE). This halving is not evenly distributed across the three ice sources: Greenland ice sheet mass losses would reduce by 70%, glacier mass losses by about half, and Antarctica shows no significant difference between scenarios; this is not due to a

lack of change in the Antarctica simulations themselves, but rather to the cancellation of mass gains and losses mentioned above.

Average rates of mass loss for each ice sheet and the glacier total are within 1-2 cm/century, of those of the 2013 IPCC Fifth Assessment Report²⁵ (see Methods: Comparison with IPCC assessments), and the updated assessment for RCP2.6 in the 2019 IPCC Special Report on the Oceans and Cryosphere in a Changing Climate (SROCC)¹. However, SROCC revised the projection for Antarctica under RCP8.5 up to 11 cm/century, close to the upper end of our 66% interval for SSP5-85 (though our projections may omit a commitment contribution of up to about 2 cm/century; see Methods). Our results are therefore closer to the 2013 than 2019 IPCC assessment regarding the magnitude and unclear scenario-dependence for Antarctica. Our 66% uncertainty intervals are narrower than the IPCC 66% (SROCC) and $\geq 66\%$ (AR5) uncertainty intervals, as would be expected from the latter being open-ended, except those for Greenland under SSP1-26: too few Greenland simulations were performed under low scenarios (RCP2.6, SSP1-26) to constrain the emulator variance (see Fig. 1a; Methods: 'Parameter interactions').

Emulation allows us to additionally assess the sensitivity of projections to uncertainties in their inputs as well as their robustness. If we use CMIP6 global climate models for the projections (Extended Data Figure 3), instead of FaIR, we find a slight increase in sea level contributions due to the larger proportion of models with high climate sensitivity to carbon dioxide^{33,34}: the 95th percentile increases by 7 cm under SSP5-85. We estimate the potential impact of reducing uncertainty with future knowledge by using fixed values for temperature, or for the ice sheet retreat and basal melt parameters: the width of the 5-95% ranges reduce by up to 13% and 17% respectively (tests 2-4 in Methods: Sensitivity tests; Extended Data Table 3 and Extended Data Figure 4). In other words, the ice-ocean interface is a similar magnitude contributor to, or larger, uncertainty for these projections as global warming under a particular emissions scenario. When we assess the robustness of the projections to different selections and treatments of the ice sheet simulations, we find this makes very little difference (tests 2-4 in Methods: Robustness checks; Extended Data Table 4; Extended Data Figure 5).

Antarctic focus

No clear dependence on emissions scenario emerges for Antarctica. This is partly due to the opposite scenario-dependencies of West and East Antarctica regions (Fig. 3f and g). But the average response to emissions scenario for each region is also small. A key reason is the wide variety of changes in the atmosphere and ocean in the global climate models. Figure 4 shows ice sheet model simulations where both the high and low emissions scenario were run (two climate models for Greenland, three for Antarctica). For the Greenland ice sheet, all simulations predict increased mass loss under higher emissions (Fig. 4a: red shaded region). For Antarctica, the picture is more complex, and mostly clustered according to the climate model. Many West Antarctica simulations show the same straightforward response as Greenland (Fig. 4b), particularly those that do not use the ISMIP6 basal melting parameterisation (see Methods). However, the West Antarctica simulations driven by CNRM-CM6-1 show the reverse, where mass gain through snowfall accumulation increases more under high emissions than mass loss (which is predominantly ocean-induced). (Note fewer simulations were driven by IPSL-CM5A-MR and CNRM-CM6-1 than by NorESM1-M, so their spread is necessarily smaller). East Antarctica and the Peninsula mostly also show this latter response, though some simulations show other combinations: more mass loss under low emissions than high, or mass loss under low emissions and mass gain under high.

It is challenging to evaluate which of these three climate models, or others used by ISMIP6, are most reliable for Antarctic climate change. Ocean conditions and accumulation show large spatio-temporal variability and are sparsely observed; models imperfectly represent important processes, and it is unclear whether the newer CMIP6 models have improved relative to CMIP5^{13,35-38}. Most of the climate models were from CMIP5, including NorESM1-M and IPSL-CM5A-MR, and were selected by their success at reproducing southern climatological observations (while also sampling a range of future climate responses)¹⁸. NorESM-1M has a lower than average atmospheric warming, hence less snowfall, while IPSL-CM5A-MR is higher than average (particularly for East Antarctica)¹⁸. The newer CMIP6 models, including CNRM-CM6-1, were selected only by their availability. Changing the selection or treatment of Antarctica simulations – e.g. using subsets of climate models, or rejecting simulations with net mass gain early in the projections – do not result in any substantial scenario-dependence (see tests 7-10 in Methods: Robustness checks; Extended Data Table 4; Extended Data Figure 5).

Uncertainty about the scenario-dependence of Antarctic projections is not new. The IPCC Fifth Assessment Report (2013) stated 'the current state of knowledge does not permit an assessment' of the dependence of rapid dynamical change on scenario. Some studies that show strong scenario-dependence neglect the compensating accumulation part^{26,39}, use extreme¹ ice shelf collapse scenarios²⁴, or the basal melt parameterisation uncertainty is the same order as, or larger than, the scenario-dependence^{27,40,41}. To be clear, we do not assert that Antarctica's future does not depend on future greenhouse emissions or global warming: only that the relationship between global and Antarctic climate change, and the ice sheet's response, are complex, only partially understood, and involve compensating factors of increasing mass loss and gain which result in a balance we are not yet confident about.

We test the sensitivity of the Antarctica projections to the basal melting parameter. The main projections combine two distributions¹³ for γ derived from observations of mean Antarctic basal melt rates or the ten highest melt rates for Pine Island Glacier (see Methods). Using the mean distribution decreases the median to ~0 cm SLE and the 95th percentile to ~8 cm SLE for all scenarios; using the high distribution has less effect, increasing the median to 6 cm SLE and the 95th percentile to ~16 cm SLE (Extended Data Table 3 and Extended Data Figure 4: tests 5 and 6). We also try and reproduce the higher projections of ref. [26] using a similar approach to sampling basal melt (see Methods), and find we only obtain similar projections when using extreme values of our parameter range (Extended Data Table 3 and Extended Data Figure 4: tests 7 and 8). This suggests ref. [26] could be interpreted as more pessimistic projections: they use values of basal melt sensitivity to ocean temperature consistent with those estimated for the Amundsen Sea region³⁹, which is currently undergoing most change.

However, other factors can lead to similarly high projections. In particular, the sensitivity of an individual ice sheet model to the basal melt parameter can have a large effect. This differs widely across ice sheet models, and also depends on the climate model (Extended Data Figure 6). Emulator projections based on a single model with high or low sensitivity are shown in Extended Data Figure 5 (tests 4 and 5; Extended Data Table 4). These also do not show strong scenario-dependence – just a 2-3 cm decrease under high emissions for the low sensitivity model, because the snowfall effect is more apparent – but instead predict a high or low sea level contribution, respectively, regardless of scenario (95th percentiles: 29-30 cm and 7-9 cm, respectively). The high sensitivity of the first model (SICOPOLIS) is probably

due to the way that sub-shelf melting is applied: over entire grid cells along the grounding line, rather than just the parts detected as floating²⁶. We also show results from the four most sensitive models, which are similarly high (Extended Data Table 4 and Extended Data Figure 5: test 6). We do not have sufficient observations to evaluate which ice sheet models have the most realistic response, nor sufficient understanding to confidently predict how basal melt sensitivity might change in future^{13,36}, and therefore use all models in the main projections (see also 'Risk-averse projections' below).

The ice shelf collapse scenario has little effect on our projections. Switching it on increases the Antarctic Peninsula and East Antarctic median contributions by 1 cm and 0-1 cm SLE from 2015-2100, with no change for West Antarctica (Extended Data Table 3 and Extended Data Figure 4: test 9-10). This is similar, within uncertainties, to the ice sheet simulations (Extended Data Figure 7). The effect is small because surface meltwater is not projected to be enough to cause collapses until the second half of the century, and even then only for small number of shelves, mostly around the Peninsula¹⁵. Some combinations of climate and ice sheet models do project larger sea level contributions – in particular, 5 cm for East Antarctica from the SICOPOLIS ice sheet model driven by HadGEM2-ES. The HadGEM2-ES climate model projects extreme ocean warming in the Ross Sea¹⁸, while SICOPOLIS has one of the largest responses among the ice sheet models (as described above). If these two were found to be the most realistic models, then the ISMIP6 ensemble and emulator may underestimate the effect of ice shelf collapse by a few centimetres. Further results are in the Methods ('Parameter interactions').

Risk-averse projections

Given the wide range and cancellations of responses across models and parameters, we present alternative 'pessimistic but physically plausible' Antarctica projections for risk-averse stakeholders, by combining a set of assumptions that lead to high sea level contributions. These are: the four ice sheet models most sensitive to basal melting; the four climate models that lead to highest Antarctic sea level contributions, and the one used to drive most of the ice shelf collapse simulations; the high basal melt (Pine Island Glacier) distribution; and with ice shelf collapse 'on' (i.e. combining robustness tests 6 and 7 and sensitivity tests 6 and 10). This storyline would come about if the high basal melt sensitivities currently observed at Pine Island Glacier soon become widespread around the continent; the ice sheet responds to these

with extensive retreat and rapid ice flow; and atmospheric warming is sufficient to disintegrate ice shelves, but does not substantially increase snowfall. The risk-averse projections are more than five times the main estimates: median 21 cm (95th percentile range 7 to 43 cm) under the NDCs (Fig. 3j), and essentially the same under SSP5-85 (Table 1; regions shown in Extended Data Figure 4: test 11), with the 95th percentiles emerging above the main projections after 2040 (Fig. 3d). This is very similar to projections²⁴ under an extreme scenario of widespread ice shelf collapses for RCP8.5 (median 21 cm; 95th percentile range 9 to 39 cm). The median is higher than ref. [26] for RCP8.5, though the 95th percentile is smaller. No models that include a representation of rapid ice cliff collapse through the proposed 'Marine Ice Cliff Instability'⁴³ mechanism participated in ISMIP6. This hypothesis is the process with the largest estimated systematic impact on projections: it could increase projections by tens of centimetres, if both the mechanism and projections of extreme ice shelf collapse are found to be robust^{24,44}.

Our risk-averse Antarctica projections increase the total land ice sea level contribution to 42 cm (95th percentile 25 to 67 cm) SLE under current policies and pledges (NDCs), and to 30 cm (95th percentile 12 to 56 cm) SLE even under SSP1-19. This means that plausible modelling choices for Antarctica could change the median land ice contribution by more (17 cm SLE) than the difference between these emissions scenarios (12 cm SLE). This ambiguity limits confidence in assessing the effectiveness of mitigation on the response of global land ice to climate change. When combined, the effects of uncertain emissions and Antarctic response lead to a threefold spread in median projections of the land ice contribution to sea level rise, ranging from 13 to 42 cm SLE over 2015-2100, implying that flexible adaptation under substantial uncertainty will be essential until either can be further constrained.

Not all modelling uncertainties could be systematically assessed here. Aside from the ice cliff instability hypothesis, these include ice sheet basal hydrology and sliding; glacier model parameters, ice-water interactions, and meltwater routing; model initialisation; and the use of coarse resolution global climate models (and a single high-resolution regional model for the Greenland ice sheet). The probabilities we present are therefore specific to our ensembles, and adding new climate and ice sheet models, or exploration of new parameters, could shift or broaden their distributions⁴⁵. However, our projections demonstrate the importance of systematic design to assess as many uncertainties as feasible, and represent the current state-of-the art in estimating the land ice contribution to global mean sea level rise.

Sea level contribution from 2015-2100 (cm SLE)	Main projections		Risk-averse projections	
	50 [5, 95]% percentiles	[17, 83]% percentiles	50 [5, 95]% percentiles	[17, 83]% percentiles
Global glaciers				
SSP119	7 [4, 10]	[5, 9]		
SSP126	8 [5, 12]	[6, 10]		
SSP245	11 [7, 15]	[9, 13]		
NDCs	13 [9, 18]	[11, 16]		
SSP370	14 [10, 19]	[12, 17]		
SSP585	16 [12, 21]	[14, 19]		
Greenland ice sheet				
SSP1-19	2 [-6, 11]	[-2, 7]		
SSP1-26	3 [-4, 12]	[-1, 8]		
SSP2-45	5 [-2, 14]	[1, 10]		
NDCs	7 [0, 16]	[3, 12]		
SSP3-70	8 [0, 17]	[4, 13]		
SSP5-85	10 [2, 20]	[5, 15]		
Antarctic ice sheet				
SSP1-19	4 [-5, 14]	[-1, 10]	21 [6, 42]	[12, 32]
SSP1-26	4 [-5, 14]	[-1, 10]	21 [7, 43]	[12, 31]
SSP2-45	4 [-5, 14]	[-1, 9]	21 [7, 43]	[12, 31]
NDCs	4 [-5, 14]	[-1, 10]	21 [7, 43]	[13, 31]
SSP3-70	4 [-5, 14]	[-1, 10]	21 [8, 43]	[13, 31]
SSP5-85	4 [-5, 14]	[-1, 10]	22 [8, 43]	[14, 32]
Land ice				
SSP1-19	13 [0, 28]	[6, 21]	30 [12, 56]	[20, 43]
SSP1-26	16 [3, 30]	[8, 24]	33 [15, 58]	[22, 45]
SSP2-45	20 [7, 35]	[13, 28]	38 [20, 63]	[28, 50]
NDCs	25 [11, 40]	[17, 33]	42 [25, 67]	[32, 54]
SSP3-70	27 [13, 41]	[19, 35]	44 [27, 70]	[34, 56]
SSP5-85	30 [16, 46]	[22, 39]	48 [30, 75]	[38, 61]

374

375 **Acknowledgements**

376 We thank Jonathan Rougier for generously providing advice and support throughout, and
377 writing the original random effects model. We also thank Baylor Fox-Kemper, Helene
378 Hewitt, Robert Kopp, Sybren Drijfhout and Jeremy Rohmer for useful discussions,
379 suggestions and support. We thank Daniel Williamson, Nicholas Barrand and two
380 anonymous referees for their thorough and constructive comments, which greatly improved
381 the manuscript. We thank the Climate and Cryosphere (CliC) effort, which provided support
382 for ISMIP6 and GlacierMIP through sponsoring of workshops, hosting the websites and
383 ISMIP6 wiki, and promotion. We acknowledge the World Climate Research Programme,
384 which, through its Working Group on Coupled Modelling, coordinated and promoted CMIP5
385 and CMIP6. We thank the climate modeling groups for producing and making available their
386 model output, the Earth System Grid Federation (ESGF) for archiving the CMIP data and
387 providing access, the University at Buffalo for ISMIP6 data distribution and upload, and the
388 multiple funding agencies who support CMIP5 and CMIP6 and ESGF. We thank the ISMIP6
389 steering committee, the ISMIP6 model selection group and the ISMIP6 dataset preparation
390 group for their continuous engagement in defining ISMIP6. This is ISMIP6 contribution No.
391 13. This publication was supported by PROTECT, which has received funding from the
392 European Union's Horizon 2020 research and innovation programme under grant agreement
393 No 869304. This is PROTECT contribution number XX.

394

395 Individual author acknowledgements follow. Tamsin Edwards was supported by PROTECT
396 and the UK Natural Environment Research Council grant NE/T007443/1. Fiona Turner was
397 supported by PROTECT. James O'Neill was supported by the UK Natural Environment
398 Research Council London Doctoral Training Partnership. Rupert Gladstone's contribution
399 was supported by Academy of Finland grants 286587 and 322430. William Lipscomb and
400 Gunter Leguy were supported by the National Center for Atmospheric Research, which is a
401 major facility sponsored by the National Science Foundation under Cooperative Agreement
402 No. 1852977. Computing and data storage resources for CISM simulations, including the
403 Cheyenne supercomputer (doi:10.5065/D6RX99HX), were provided by the Computational
404 and Information Systems Laboratory (CISL) at NCAR. Support for Xylar Asay-Davis,
405 Matthew J. Hoffman, Stephen Price, and Tong Zhang was provided through the Scientific
406 Discovery through Advanced Computing (SciDAC) program funded by the US Department

407 of Energy (DOE), Office of Science, Advanced Scientific Computing Research and
 408 Biological and Environmental Research Programs. Nicholas R. Golledge, Daniel P. Lowry
 409 and Brian Anderson were supported by NZ Ministry for Business, Innovation and
 410 Employment contracts RTUV1705 ('NZSeaRise') and ANTA1801 ('Antarctic Science
 411 Platform'). Jonathan Gregory and Robin S. Smith were supported by the National Centre for
 412 Atmospheric Science, funded by the UK National Environment Research Council. Reinhard
 413 Calov was funded by the PalMod project of the Bundesministerium für Bildung und
 414 Forschung (BMBF) with the grants FKZ 01LP1502C and 01LP1504D. Daniel Martin and
 415 Courtney Shafer were supported by the Director, Office of Science, Offices of Advanced
 416 Scientific Computing Research (ASCR) and Biological and Environmental Research (BER),
 417 of the U.S. Department of Energy under Contract No. DE-AC02-05CH11231, as a part of the
 418 ProSpect SciDAC Partnership. BISICLES simulations used resources of the National Energy
 419 Research Scientific Computing Center (NERSC), a U.S. Department of Energy Office of
 420 Science User Facility operated under Contract No. DE-AC02-05CH11231. Chen Zhao and
 421 Ben Galton-Fenzi were supported under the Australian Research Council's Special Research
 422 Initiative for Antarctic Gateway Partnership (Project ID SR140300001) and received grant
 423 funding from the Australian Government for the Australian Antarctic Program Partnership
 424 (Project ID ASCI000002). Work was performed by Eric Larour, Nicole Schlegel, and Helene
 425 Seroussi at the California Institute of Technology's Jet Propulsion Laboratory under a
 426 contract with the National Aeronautics and Space Administration's Cryosphere, Sea Level
 427 Change Team, and Modeling, Analysis and Prediction (MAP) Programs. They acknowledge
 428 computational resources and support from the NASA Advanced Supercomputing Division.
 429 The CMIP5 and CMIP6 projection data were processed by Christine McKenna with funding
 430 from the European Union's CONSTRAIN project as part of the Horizon 2020 Research and
 431 Innovation Programme under grant agreement number 820829. Alice Barthel was supported
 432 by the DOE Office of Science HiLAT-RASM project and Early Career Research program.
 433 Helene Seroussi was supported by grants from NASA Cryospheric Science, Sea Level
 434 Change Team, and Modeling, Analysis, and Predictions Programs. Torsten Albrecht and
 435 Ricarda Winkelmann are supported by the Deutsche Forschungsgemeinschaft (DFG) in the
 436 framework of the priority program "Antarctic Research with comparative investigations in
 437 Arctic ice areas" by grants WI4556/2-1 and WI4556/4-1, and within the framework of the
 438 PalMod project (FKZ: 01LP1925D) supported by the German Federal Ministry of Education
 439 and Research (BMBF) as a Research for Sustainability initiative (FONA). Ronja Reese is

supported by the Deutsche Forschungsgemeinschaft (DFG) by grant WI4556/3-1 and through the TiPACCs project that receives funding from the European Union's Horizon 2020 Research and Innovation program under grant agreement no. 820575. Ralf Greve and Christopher Chambers were supported by Japan Society for the Promotion of Science (JSPS) KAKENHI grant Nos. JP16H02224 and JP17H06323. Ralf Greve was supported by JSPS KAKENHI grant No. JP17H06104, by a Leadership Research Grant of Hokkaido University's Institute of Low Temperature Science (ILTS), and by the Arctic Challenge for Sustainability (ArCS) project of the Japanese Ministry of Education, Culture, Sports, Science and Technology (MEXT) (program grant number JPMXD1300000000). Frank Pattyn and Sainan Sun were supported by the MIMO project within the STEREO III programme of the Belgian Science Policy Office, contract SR/00/336 and the Fonds de la Recherche Scientifique (FNRS) and the Fonds Wetenschappelijk Onderzoek-Vlaanderen (FWO) under the EOS Project number O0100718F. Andrew Shepherd was supported by the UK Natural Environment Research Council in partnership with the Centre for Polar Observation and Modelling and the British Antarctic Survey and by the European Space Agency Climate Change Initiative. Denis Felikson was supported by an appointment to the NASA Postdoctoral Program at the NASA Goddard Space Flight Center, administered by Universities Space Research Association under contract with NASA.

Author contributions

T.L.E. conceived the idea, carried out all statistical analysis except the random effects model, produced the figures, and wrote the manuscript. S.N. led ISMIP6, including experimental design, organisation and analysis, and provided scientific interpretation. B.M and R.H. co-led GlacierMIP and contributed simulations (below), and provided data and interpretation. H. G. and H.S. led the processing and analysis in ISMIP6 for the Greenland and Antarctic ice sheets, respectively, contributed simulations (below), and provided scientific interpretation and advice. N.J. and D.S. co-derived with T.L.E. the ice sheet continuous parameter distributions for the emulator, and also derived the corresponding ocean forcing parameterisation studies with X.A.-D. and T.H. for Antarctica and F.S., D.F. and M.M. for Greenland. F.T. performed the random effects model cross-check for Antarctica. C.S. provided the FaIR projections and C.M. provided the CMIP5 and CMIP6 projection data for the emulator. E.S. led the ISMIP6 data processing. A.A.O., J.M.G., E.L., W.H.L., A.J.P.,

A.S. contributed to the ISMIP6 experimental design, organisation and analysis as members of
 its steering committee, and R.S and W.H.L. led the ISMIP6 atmosphere focus group. C.M.L.,
 A.B. and C.A. selected the CMIP5 models for ISMIP6, X.F. and P.A. ran the surface mass
 balance model for the Greenland and R.Cu. prepared the Antarctic surface mass balance, and
 L.D.T. and M.v.d.B. provided the ice shelf collapse forcing. For Antarctica: T.K. and A.H.
 contributed the AWI/PISM simulations; M.H., T.Z. and S.P. contributed the DOE/MALI
 simulations; R.G. and R.Ca. contributed the ILTS_PIK/SICOPOLIS simulations; H.G. and
 R.v. d. W. contributed the IMAU/IMAUICE simulations; N.-J.S. and H.S. contributed the
 JPL/ISSM simulations; C.D. and A.Q. contributed the LSCE/GRISLI simulations; G.L. and
 W.L. contributed the NCAR/CISM simulations; R.R., T.A. and R.W. contributed the
 PIK/PISM simulations;. T.P., M.M. and H.S. contributed the UCIJPL/ISSM simulations; F.P.
 and S.S. contributed the ULB/fETISH simulations; C.Z., R.G., B.G-F. and T.Z. contributed
 the UTAS/Elmer/Ice simulations; J.V.B. and P.H. contributed the VUB/AISMPALEO
 simulations; N.R.G. and D.L. contributed the VUW/PISM simulations; and D.F.M. and C.S.
 contributed the CPOM/BISICLES simulations. For Greenland: M.R. and A.H. contributed
 the AWI/ISSM simulations; V.L. and A.J.P. contributed the BGC/BISICLES simulations;
 I.N., D.F. and S.N. contributed the GSFC/ISSM simulations; R.G., R.Ca. and C.C.
 contributed the ILTS_PIK/SICOPOLIS simulations; H.G., R.v.d.W. and M.v.d.B. contributed
 the IMAU/IMAUICE simulations; N.-J.S. and H.S. contributed the JPL/ISSM simulations;
 J.C. and N.-J.S. contributed the JPL/ISSMPALEO simulations; A.Q. and C.D. contributed
 the LSCE/GRISLI simulations; L.T. contributed the MUN/GSM simulations; W.H.L. and
 G.R.L. contributed the NCAR/CISM simulations; A.A contributed the UAF/PISM
 simulations; Y.C., H.S. and M.M. contributed the UCIJPL/ISSM simulations; S.L.c. and P.H.
 contributed the VUB/GISM simulations; and D.P.L. and N.R.G. contributed the VUW/PISM
 simulations. For global glaciers: B.A. contributed the AND2012 simulations; K.F. and A.S.
 contributed the GLIMB simulations; M.H. contributed the GloGEM simulations; H.Z.
 contributed the GloGEMflow simulations; S.S. contributed the JULES simulations; P.K. and
 W.I. contributed the KRA2017 simulations; B.M. and J.M. contributed the MAR2012
 simulations; F.M. and N.C. contributed the OGGM simulations; D.R. and R.H. contributed
 the PyGEM simulations; A.B. and V.R. contributed the RAD2014 simulations; R.v.d.W.
 contributed the WAL2001 simulations; and A. Bl. and J.-H. M. assisted with data handling.
 All authors contributed to the manuscript.

References

1. Oppenheimer, M. *et al.* in *IPCC Special Report on the Ocean and Cryosphere in a Changing Climate* (eds. Portner, H. O. *et al.*) (2019).
2. Nowicki, S. M. J. *et al.* Ice Sheet Model Intercomparison Project (ISMIP6) contribution to CMIP6. *Geoscientific Model Development* 9, 4521–4545 (2016).
3. Nowicki, S. *et al.* Experimental protocol for sea level projections from ISMIP6 stand-alone ice sheet models. *The Cryosphere*, 14, 2331–2368, <https://doi.org/10.5194/tc-14-2331-2020>, 2020.
4. Eyring, V. *et al.* Overview of the Coupled Model Intercomparison Project Phase 6 (CMIP6) experimental design and organization. *Geoscientific Model Development* 9, 1937–1958 (2016).
5. Hock, R. *et al.* GlacierMIP – A model intercomparison of global-scale glacier mass-balance models and projections. *Journal of Glaciology* 65, 453–467 (2019).
<https://doi.org/10.1017/jog.2019.22>
6. Goelzer, H. *et al.* Design and results of the ice sheet model initialisation experiments initMIP-Greenland: an ISMIP6 intercomparison. *The Cryosphere* 12, 1433–1460 (2018).
7. Seroussi, H. *et al.* initMIP-Antarctica: an ice sheet model initialization experiment of ISMIP6. *The Cryosphere* 13, 1441–1471 (2019).
8. Marzeion, B. *et al.* Partitioning the Uncertainty of Ensemble Projections of Global Glacier Mass Change. *Earth's Future*, 8(7), e2019EF001470 (2020).
9. van Vuuren, D. P. *et al.* The representative concentration pathways: an overview. *Climatic Change* 109, 5–31 (2011).
10. Slater, D. A. *et al.* Estimating Greenland tidewater glacier retreat driven by submarine melting. *The Cryosphere* 13, 2489–2509 (2019).
11. Slater, D. A. *et al.* Twenty-first century ocean forcing of the Greenland ice sheet for modelling of sea level contribution, *The Cryosphere*, 14, 985–1008,
<https://doi.org/10.5194/tc-14-985-2020>, 2020.
12. Favier, L. *et al.* Assessment of sub-shelf melting parameterisations using the ocean–ice-sheet coupled model NEMO(v3.6)–Elmer/Ice(v8.3). *Geoscientific Model Development* 12, 2255–2283 (2019).
13. Jourdain, N. C. *et al.* A protocol for calculating basal melt rates in the ISMIP6 Antarctic ice sheet projections, *The Cryosphere*, 14, 3111–3134,
<https://doi.org/10.5194/tc-14-3111-2020>, 2020.
14. Goelzer, H. *et al.* The future sea-level contribution of the Greenland ice sheet: a multi-model ensemble study of ISMIP6. *The Cryosphere*, 14, 3071–3096,
<https://doi.org/10.5194/tc-14-3071-2020> (2020).
15. Seroussi, H. *et al.* ISMIP6 Antarctica: a multi-model ensemble of the Antarctic ice sheet evolution over the 21st century. *The Cryosphere*, 14, 3033–3070,
<https://doi.org/10.5194/tc-14-3033-2020> (2020).
16. Nowicki, S. *et al.* Contrasting contributions to future sea level under CMIP5 and CMIP6 scenarios from the Greenland and Antarctic ice sheets. *Geophysical Research Letters*, in review.
17. Goelzer, H. *et al.* Remapping of Greenland ice sheet surface mass balance anomalies for large ensemble sea-level change projections. *The Cryosphere*, 14, 1747–1762,
<https://doi.org/10.5194/tc-14-1747-2020>, 2020.
18. Barthel, A. *et al.* CMIP5 model selection for ISMIP6 ice sheet model forcing: Greenland and Antarctica, *The Cryosphere*, 14, 855–879, <https://doi.org/10.5194/tc-14-855-2020>, 2020.

- 556 19. Riahi, K. *et al.* The Shared Socioeconomic Pathways and their energy, land use, and
557 greenhouse gas emissions implications: An overview. *Global Environmental Change*
558 42, 153–168 (2017).
- 559 20. O'Neill, B. C. *et al.* The Scenario Model Intercomparison Project (ScenarioMIP) for
560 CMIP6. *Geoscientific Model Development* 9, 3461–3482 (2016).
- 561 21. Taylor, K. E., Stouffer, R. J. & Meehl, G. A. An Overview of CMIP5 and the
562 Experiment Design. *B Am Meteorol Soc* 93, 485–498 (2012).
- 563 22. Andrianakis, I. & Challenor, P. G. The effect of the nugget on Gaussian process
564 emulators of computer models. *Computational Statistics & Data Analysis* 56, 4215–
565 4228 (2012).
- 566 23. Gramacy, R. B. & Lee, H. K. H. Cases for the nugget in modeling computer
567 experiments. *Stat Comput* 22, 713–722 (2010).
- 568 24. Edwards, T. L. *et al.* Revisiting Antarctic ice loss due to marine ice cliff instability.
569 *Nature* 566, 58–64 (2019).
- 570 25. Church, J.A., P.U. Clark, A. Cazenave, J.M. Gregory, S. Jevrejeva, A. Levermann,
571 M.A. Merrifield, G.A. Milne, R.S. Nerem, P.D. Nunn, A.J. Payne, W.T. Pfeffer, D.
572 Stammer and A.S. Unnikrishnan, 2013: Sea Level Change. In: *Climate Change 2013:*
573 *The Physical Science Basis. Contribution of Working Group I to the Fifth Assessment*
574 *Report of the Intergovernmental Panel on Climate Change* [Stocker, T.F., D. Qin, G.-
575 K. Plattner, M. Tignor, S.K. Allen, J. Boschung, A. Nauels, Y. Xia, V. Bex and P.M.
576 Midgley (eds.)]. Cambridge University Press, Cambridge, United Kingdom and New
577 York, NY, USA.
- 578 26. Levermann, A. *et al.* Projecting Antarctica's contribution to future sea level rise from
579 basal ice shelf melt using linear response functions of 16 ice sheet models (LARMIP-
580 2). *Earth Syst. Dynam.* 11, 35–76 (2020).
- 581 27. Bulthuis, K. *et al.*, Uncertainty quantification of the multi-centennial response of the
582 Antarctic ice sheet to climate change, *The Cryosphere*, 13, 1349–1380,
583 <https://doi.org/10.5194/tc-13-1349-2019>, 2019.
- 584 28. Nauels, A. *et al.*, Synthesizing long-term sea level rise projections – the MAGICC sea
585 level model v2.0. *Geosci. Model Dev.*, 10, 2495–2524 (2017)
- 586 29. Palmer, M. D., *et al.* (2020). Exploring the drivers of global and local sea-level change
587 over the 21st century and beyond. *Earth's Future*, 8, e2019EF001413. [https://doi.org/](https://doi.org/10.1029/2019EF001413)
588 [10.1029/2019EF001413](https://doi.org/10.1029/2019EF001413)
- 589 30. McKenna, C. M. *et al.*, Stringent mitigation substantially reduces risk of unprecedented
590 near-term warming rates, *Nature Climate Change*, in press.
- 591 31. Farinotti, D. *et al.*, A consensus estimate for the ice thickness distribution of all
592 glaciers on Earth, *Nature Geoscience*, 12, 168–173 (2019).
- 593 32. Biemans *et al.* (2019) Importance of snow and glacier meltwater for agriculture on the
594 Indo-Gangetic Plain, *Nature Sustainability* 2, 594–601
- 595 33. Forster, P. M., Maycock, A. C., McKenna, C. M. & Smith, C. J. Latest climate models
596 confirm need for urgent mitigation. *Nature Climate Change* 1–4 (2019).
597 doi:10.1038/s41558-019-0660-0
- 598 34. Meehl, G. *et al.* (2020) Context for interpreting equilibrium climate sensitivity and
599 transient climate response from the CMIP6 Earth system models, *Sci. Adv.*, 6 :
600 eaba1981
- 601 35. Meredith, M. *et al.* in *IPCC Special Report on the Ocean and Cryosphere in a*
602 *Changing Climate* (eds. Portner, H. O. *et al.*) (2019).
- 603 36. Naughten, K. A. *et al.* Future Projections of Antarctic Ice Shelf Melting Based on
604 CMIP5 Scenarios. *J Climate* 31, 5243–5261 (2018).

37. Mottram, R., Hansen, N., Kittel, C., van Wessem, M., Agosta, C., Amory, C., Boberg, F., van de Berg, W. J., Fettweis, X., Gossart, A., van Lipzig, N. P. M., van Meijgaard, E., Orr, A., Phillips, T., Webster, S., Simonsen, S. B., and Souverijns, N.: What is the Surface Mass Balance of Antarctica? An Intercomparison of Regional Climate Model Estimates, *The Cryosphere Discuss.*, <https://doi.org/10.5194/tc-2019-333>, in review, 2020.
38. Roussel, M.-L., Lemonnier, F., Genthon, C., and Krinner, G.: Brief communication: Evaluating Antarctic precipitation in ERA5 and CMIP6 against CloudSat observations, *The Cryosphere*, 14, 2715–2727, <https://doi.org/10.5194/tc-14-2715-2020>, 2020.
39. Reese, R. *et al.*, The role of history and strength of the oceanic forcing in sea level projections from Antarctica with the Parallel Ice Sheet Model, *The Cryosphere*, 14, 3097–3110, <https://doi.org/10.5194/tc-14-3097-2020>, 2020.
40. Golledge, N. R. *et al.* The multi-millennial Antarctic commitment to future sea-level rise. *Nature* **526**, 421–425 (2015).
41. Golledge, N. R. *et al.* Global environmental consequences of twenty-first-century ice-sheet melt. *Nature Publishing Group* 1–23 (2019). doi:10.1038/s41586-019-0889-9
42. Levermann, A. *et al.* Projecting Antarctica's contribution to future sea level rise from basal ice shelf melt using linear response functions of 16 ice sheet models (LARMIP-2). *Earth Syst. Dynam.* 11, 35–76 (2020).
43. DeConto, R. M. & Pollard, D. Contribution of Antarctica to past and future sea-level rise. *Nature* 531, 591–597 (2016).
44. Clerc, F., Minchew, B. M. & Behn, M. D. Marine Ice Cliff Instability Mitigated by Slow Removal of Ice Shelves. *Geophysical Research Letters* 46, 12108–12116 (2019).
45. Williamson, D. B., Sansom, P. G. (2020) How are emergent constraints quantifying uncertainty and what do they leave behind? *BAMS*, 100, 2571-2588, <https://doi.org/10.1175/BAMS-D-19-0131.1>

Figure 1. Ice sheet and glacier mass loss generally increases linearly with global mean temperature. Projected mass changes from 2015-2100 in sea level equivalent (SLE) as a function of global mean surface air temperature change over the same period for (a) Greenland ice sheet, (b, c) West and East Antarctic ice sheets, (d) Greenland peripheral glaciers, (e, f) the Antarctic Peninsula and Antarctic peripheral glaciers, (g-j) four glacier regions with large maximum sea level contributions (Alaska, Arctic Canada North and South, Russian Arctic), (k, l) two regions with nonlinear temperature-dependence and total or near-total disappearance projected at high temperatures (Central Europe and Caucasus); and (m-o) three regions comprising High Mountain Asia. Central solid lines show the emulator mean, and shaded regions the mean \pm 2 s.d.. For the ice sheets (a-c, e), darker shaded regions use parameter values fixed at their default values (Greenland glacier retreat: median; Antarctic sub-shelf basal melting: median of Mean Antarctic distribution; Antarctic ice shelf collapse off), and lighter shaded regions use alternative values (Greenland: 75th percentile; Antarctica: median of Pine Island Glacier distribution). See Methods for details. Points show ice sheet and glacier simulations under RCP2.6/SSP1-26 (blue), RCP4.5 (yellow), RCP6.0 (orange) and RCP8.5/SSP5-85 (red). Solid circles for the ice sheets use the default ice-ocean parameter value and open circles use the alternative value (other simulations are not shown). Glacier

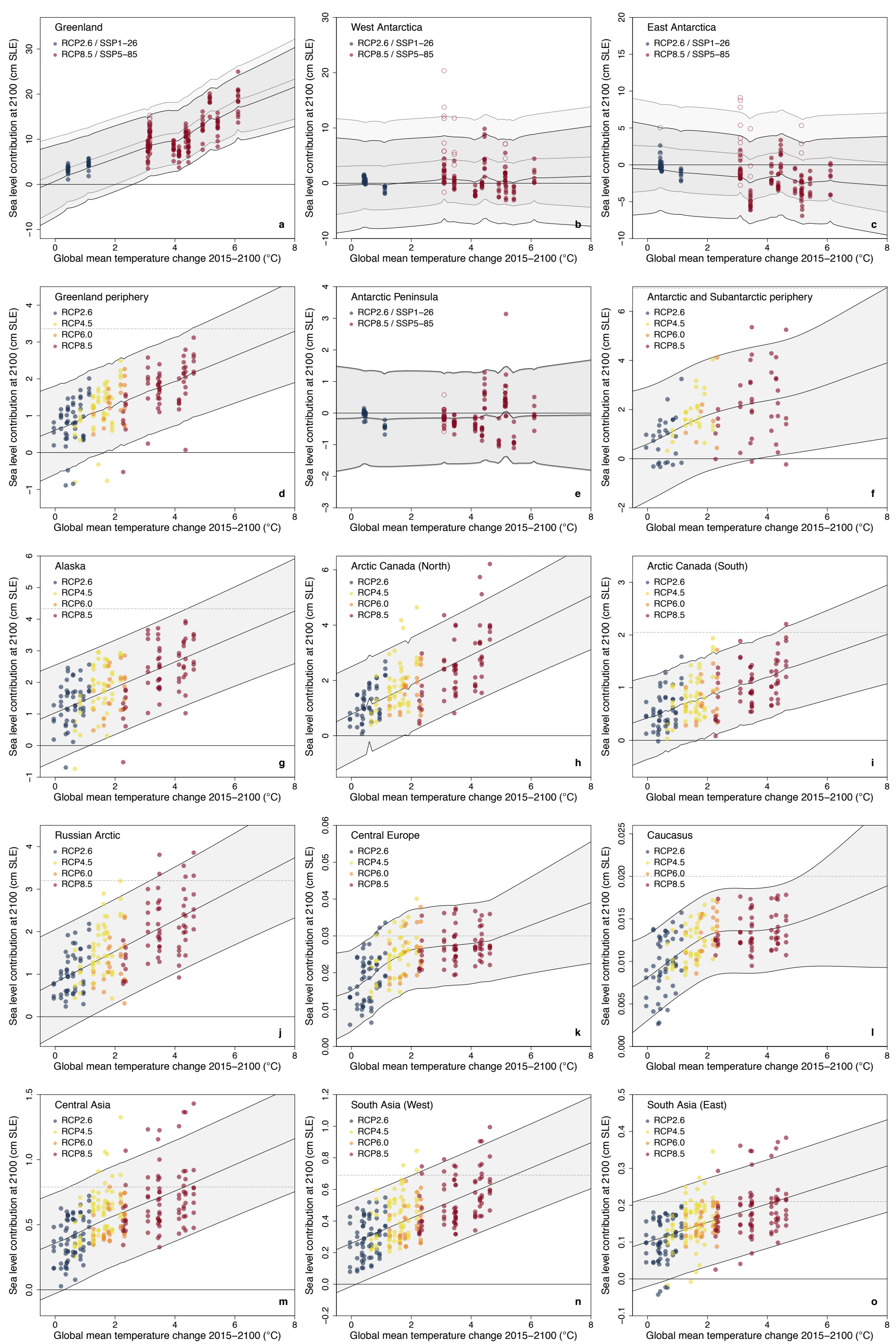
simulations are change in total volume, not volume above flotation; the estimated maximum sea level contribution (i.e. current total glacier volume above flotation)³¹ is shown (horizontal dashed line).

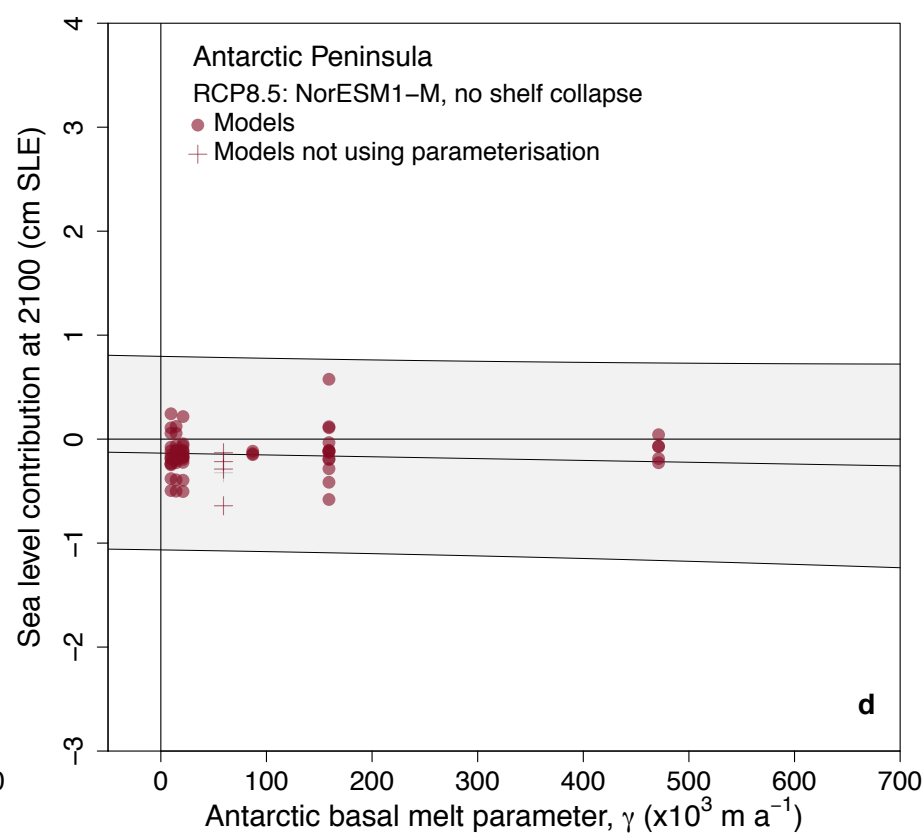
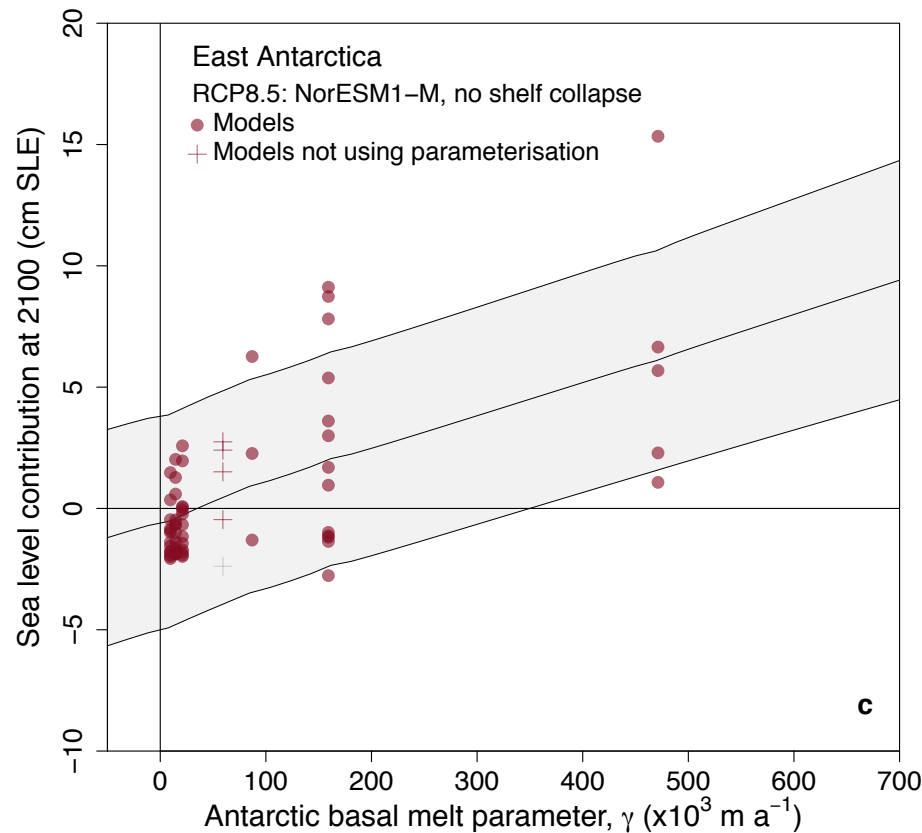
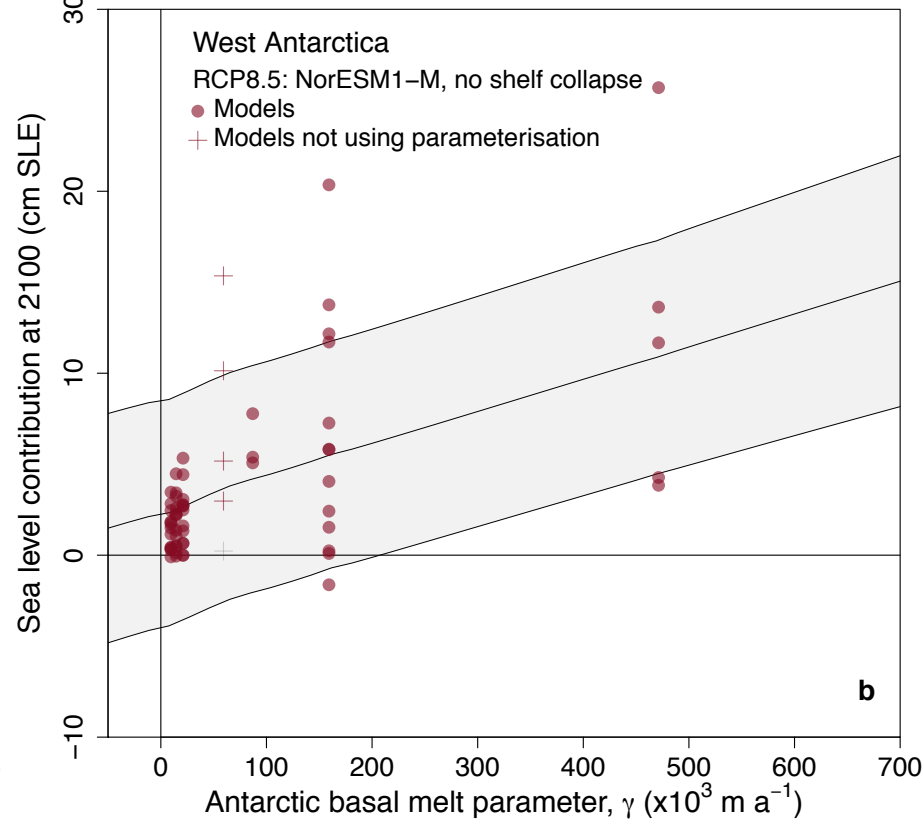
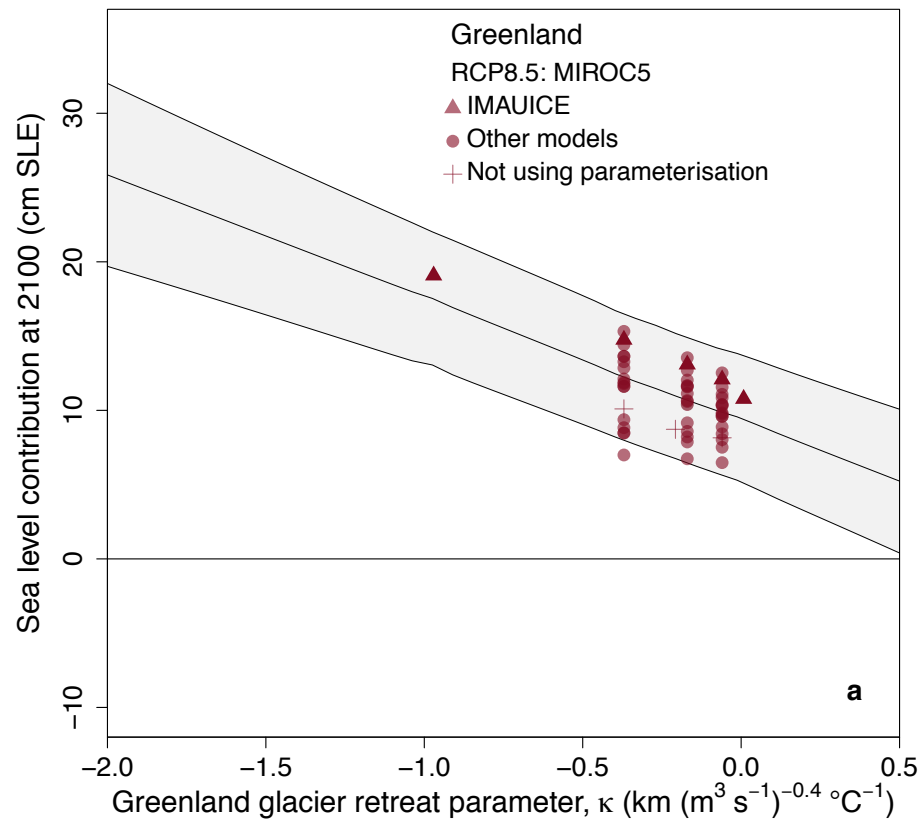
Figure 2. Ice sheet mass loss strongly depends on ice-ocean parameters. Projections of sea level contribution from 2015-2100 as a function of (a) Greenland glacier retreat parameter (κ), and basal melt parameter (γ) for (b) West Antarctica, (c) East Antarctica, (d) Peninsula. Solid line shows emulator mean estimate using fixed global temperature (projected by the global climate model most used for simulations, under RCP8.5), and shaded regions show the mean \pm 2 s.d. Symbols show ice sheet models forced by this climate model for which simulations for at least three (Greenland) or four (Antarctic) melt parameter values were available: circles use the ISMIP6 parameterisation for the ice-ocean interface; crosses use other representations, and are assigned ensemble mean values of the parameter; triangles show the Greenland ice sheet model for which two additional values of κ were run.

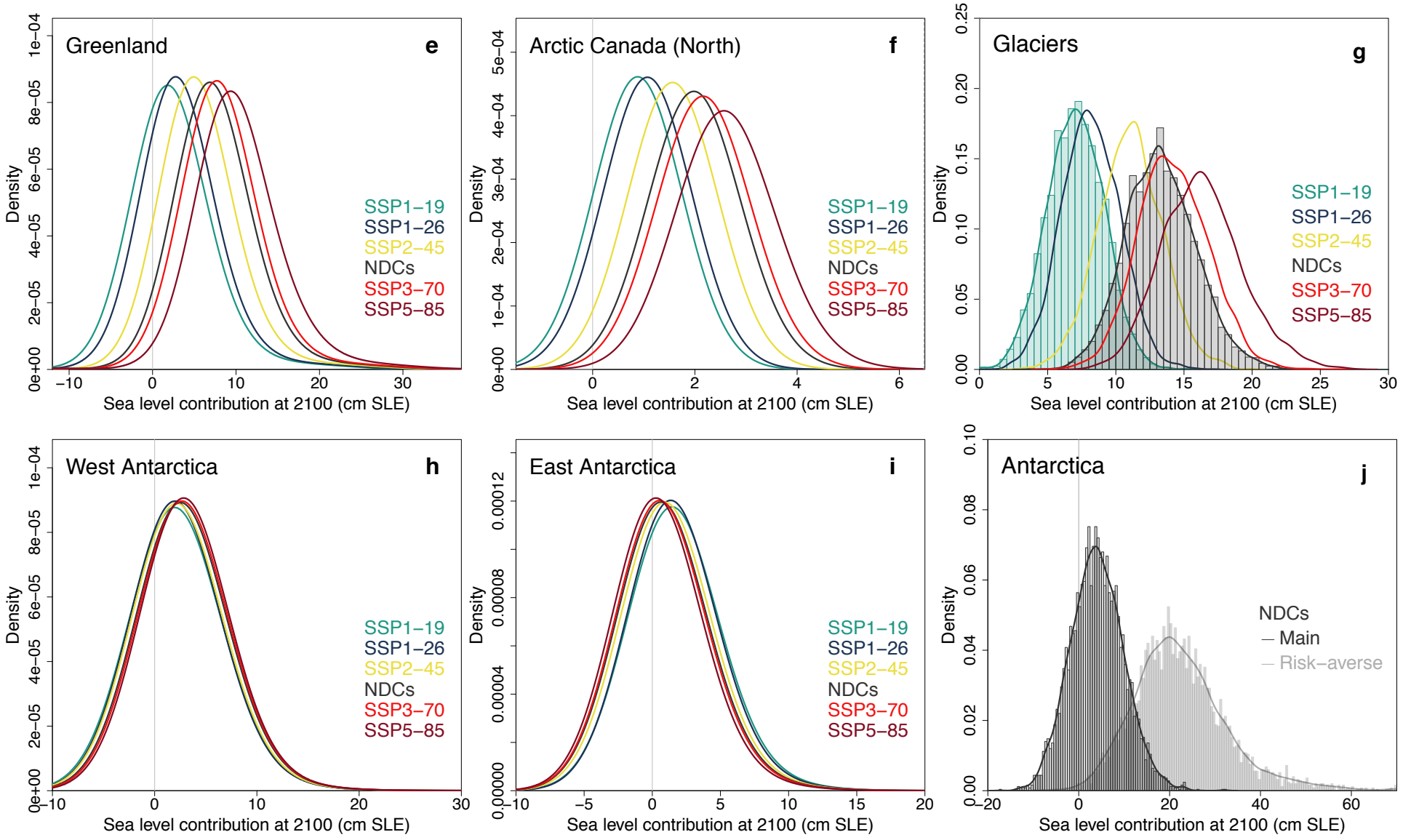
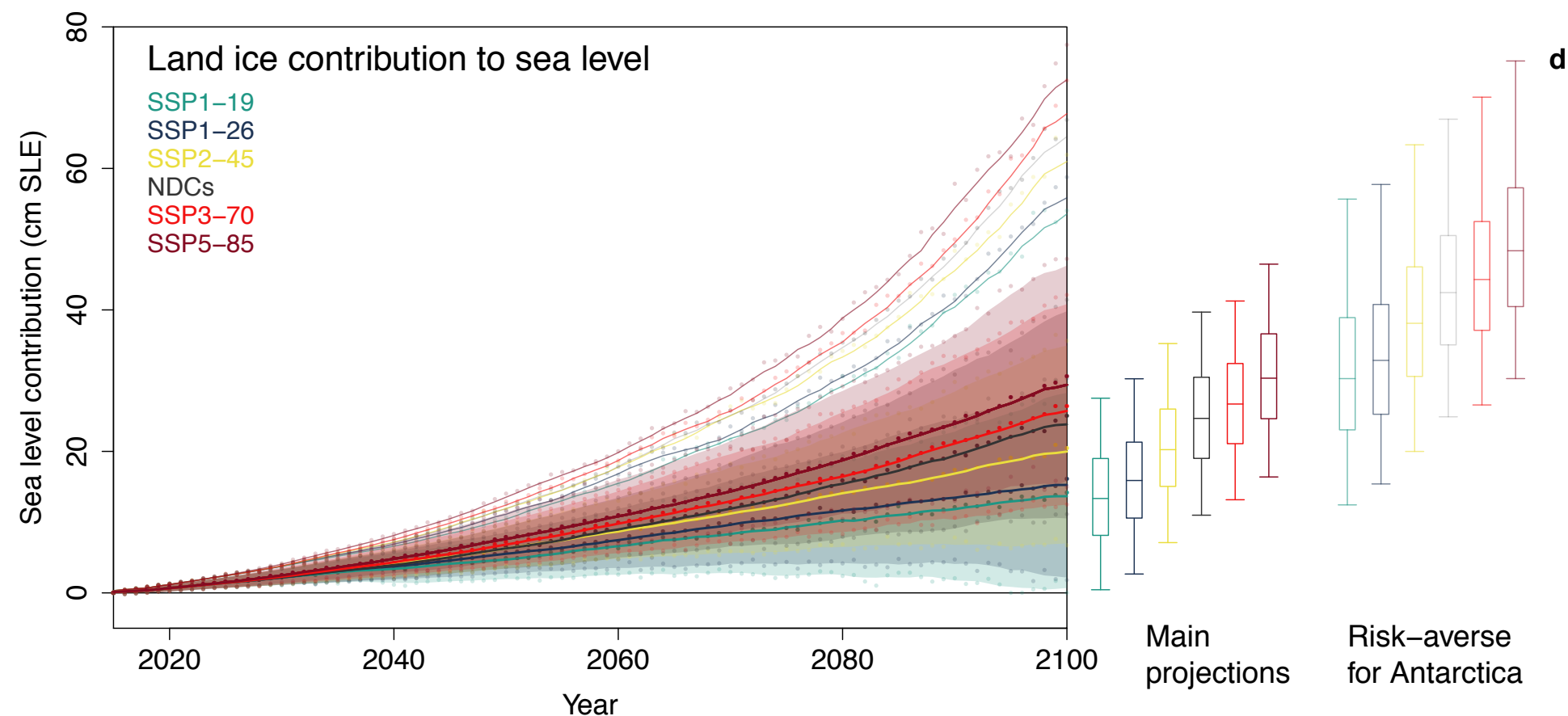
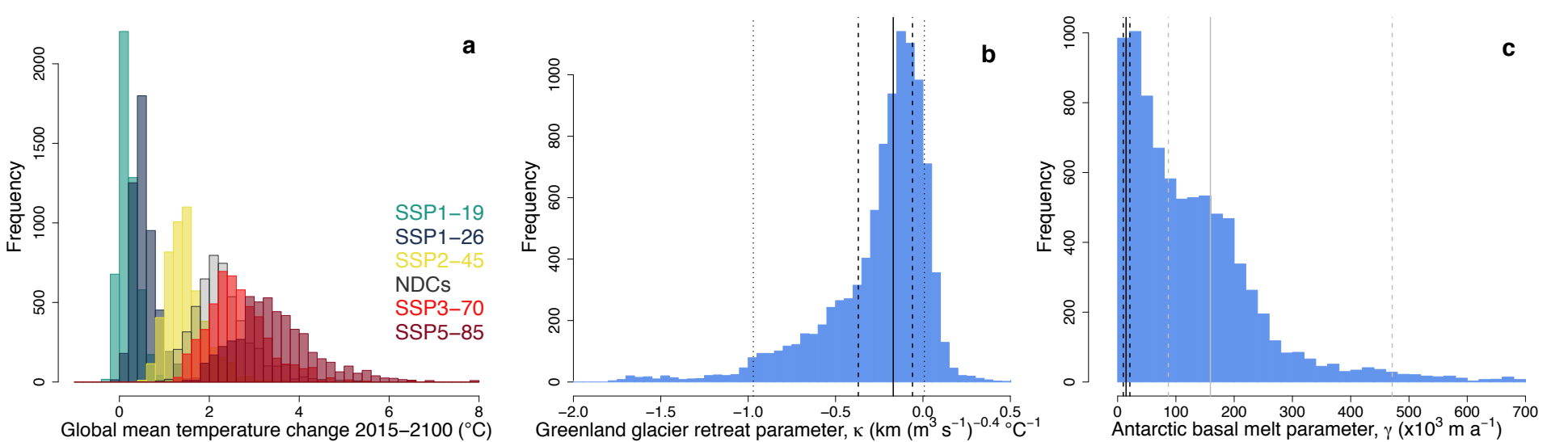
Figure 3. Projected land ice contribution to 21st century sea level rise and for selected regions at 2100. (a) Probability distributions for global mean surface air temperature change from 2015-2100 from the FaIR simple climate model under the five Shared Socioeconomic Pathways (SSPs) and current Nationally Determined Contributions (NDCs) (N = 5000 each). (b) Greenland ice sheet retreat parameter (κ) distribution (N = 10,000): vertical lines show the five values used for simulations: median (solid), 25th and 75th percentiles (dashed), and 5th and 95th percentiles (dotted). (c) Antarctic basal melt parameter (γ) distribution (N = 8200): vertical lines show the six values used for simulations: median (solid), 5th and 95th percentiles (dashed) of the Mean Antarctic (black) and Pine Island Glacier (grey) distributions (see Methods). (d) Projected land ice contribution to sea level (cm SLE) from 2015-2100 under the five SSPs and NDCs. Solid lines and shaded regions: median and 5-95th percentiles (N = 11,500 per year per scenario): 5 year smoothing applied, with original data shown as dots (interannual variation arises from annual sampling of emulator uncertainties). Pale solid lines: 95th percentiles of risk-averse projections. Box and whiskers show [5, 25, 50, 75, 95]th percentiles at 2100 (N = 115,000 per scenario) for main projections (left) and risk-averse projections for Antarctica (right). (e-j). Probability density functions for 2100 estimated for: (e) Greenland ice sheet, (f) Arctic Canada North, (g) total for glaciers, (h, i) West and East Antarctica for all scenarios, and (j) total for Antarctic ice sheet under main and risk-averse projections for the NDCs. Glacier and Antarctic totals are less smooth because they are estimated from a sum of Monte Carlo samples from each region, rather than deterministic integration (see Methods); these samples are shown for SSP1-19 and NDCs (N = 5000). Ice sheet projections do not include pre-2015 response, which is estimated to add less than 1 cm to the Greenland contribution and up to ~2 cm to the Antarctic (see Methods).

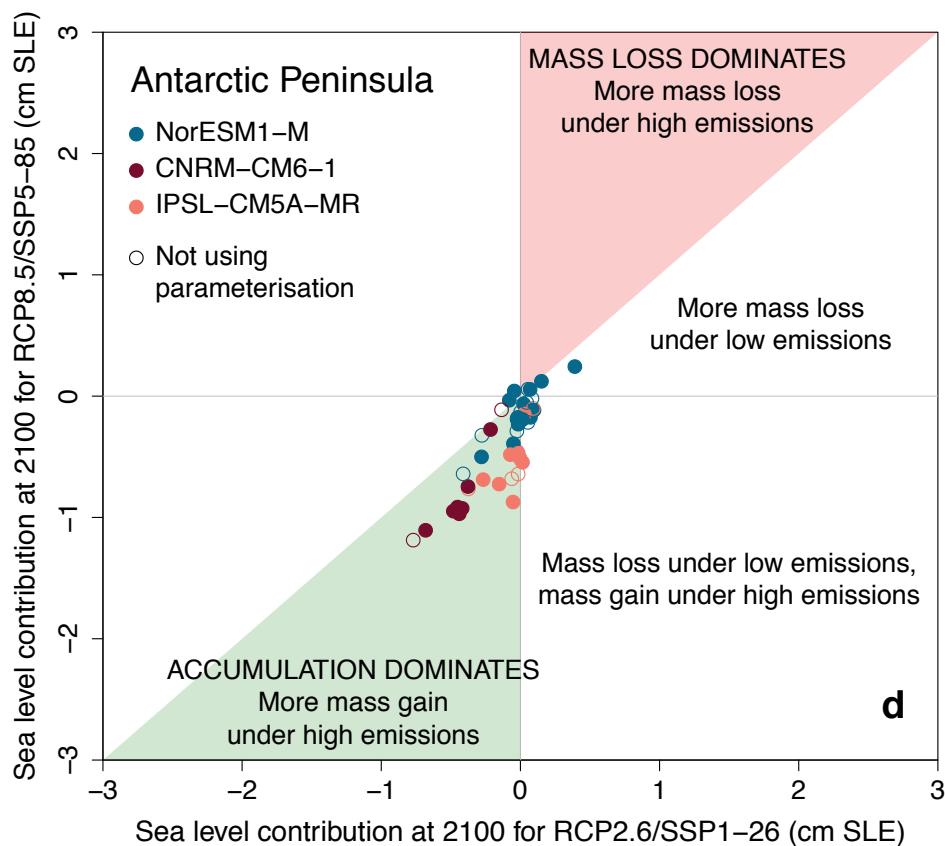
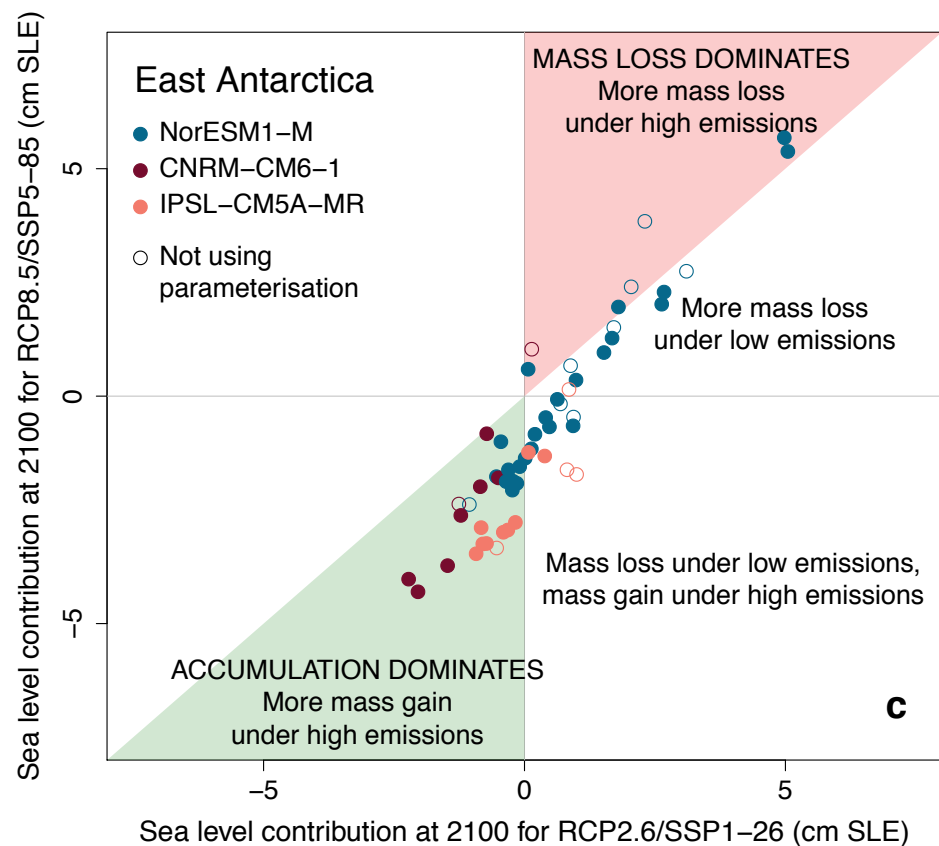
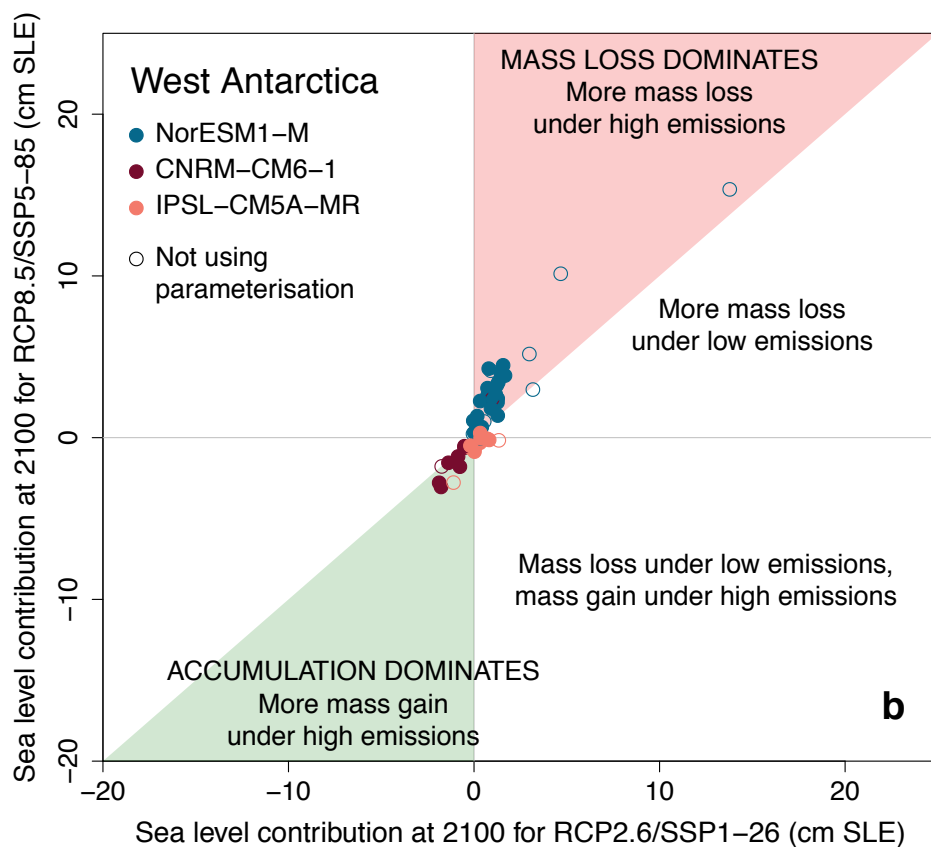
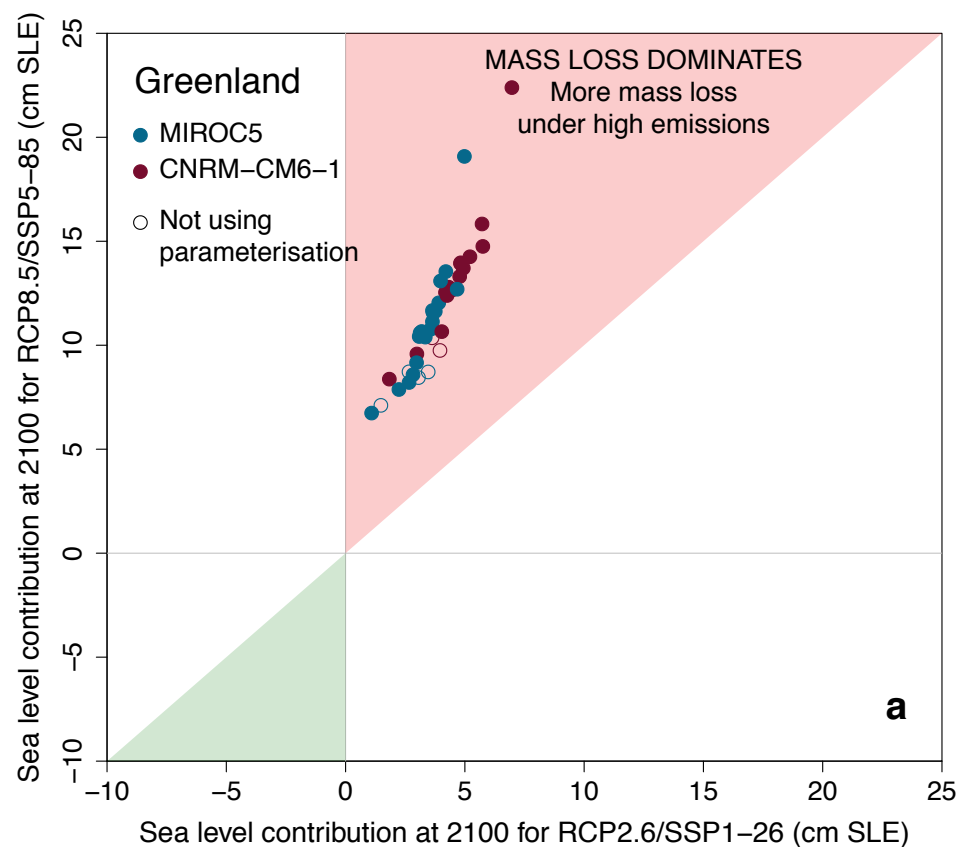
Figure 4. Climate and ice sheet projections show a wide range of responses to greenhouse gas emissions scenario. Sea level contribution at 2100 under high greenhouse gas emissions scenarios (RCP8.5 or SSP5-85) versus low scenarios (RCP2.6 or SSP1-26), categorised by climate model forcing (NorESM1-M and IPSL-CM5A-MR use RCPs; CNRM-CM6-1 use SSPs), without ice shelf collapse. a, Greenland. b, West Antarctica. c, East Antarctica. d, Antarctic Peninsula. Filled circles show ice sheet models that use the ISMIP6 parameterisations of the ice-ocean interface, while open circles show models that used their own. Simulations in the red shaded regions have more mass loss under high emissions (RCP8.5/SSP5-85) than low (RCP1-26/SSP1-26); those in the green shaded regions have more mass gain under high emissions scenarios than low. Two regions with other possible combinations are also labelled.

Table 1. Projected land ice contributions to sea level rise in 2100 under different greenhouse gas scenarios and Antarctic modelling assumptions. Projected changes to global glaciers, Greenland and Antarctic ice sheets and land ice total from 2015-2100 in sea level equivalent (cm SLE) for five Shared Socioeconomic Pathways (SSPs) and predicted emissions under the 2019 Nationally Determined Contributions (NDCs). Ice sheet projections do not include pre-2015 response, which is estimated to add less than 1 cm to the Greenland contribution and ~2 cm to the Antarctic (see Methods). The glaciers include the Greenland and Antarctic ice sheet peripheral glaciers; the overlap of Antarctic periphery glaciers with the ice sheet contribution is estimated to be less than 1 cm SLE.









Methods

Simulations

Ice sheet and glacier model simulations

Ice sheet and glacier simulations are from the Ice Sheet Model Intercomparison Project 6 (ISMIP6)^{2,3} and Glacier Model Intercomparison Project Phase 2⁸. Most are published elsewhere^{8,14-16}. Additional simulations were run for this analysis (Extended Data Table 1) as follows, where the names are group/model: 22 new Greenland experiments using [5th, 95th] percentile values of the retreat parameter under different climate model forcings with IMAU/IMAUICE1, and 113 Antarctic experiments with CPOM/BISICLES (N = 16), ILTS_PIK/SICOPOLIS (N = 31), JPL1/ISSM (N = 10), LSCE/GRISLI (N = 30) and NCAR/CISM (N = 26). Eight of the new Antarctic simulations were previous experiments described in ref. [15] using a new model (CPOM/BISICLES), and the rest (105) used 37 new combinations of previous uncertainties for additional exploration of basal melt (29) and ice shelf collapse (5) under different climate model forcings, and the interaction of ice shelf collapse and basal melt (3). CPOM/BISICLES is described in the ISMIP6 Antarctic initialisation study⁷: here the B variant is used, but with minimum resolution 1 km rather than 0.5 km. All ice sheet projections are calculated relative to a control simulation with constant present day climate (see 'Comparison with IPCC assessments' for an estimate of the 'committed' contribution this removes).

The glacier regions are listed in Extended Data Table 2 and all simulations are described in ref [8]. Greenland ice sheet projections have the peripheral glaciers (region 5) masked out, so there is no double-counting. The Antarctic periphery glaciers (region 19) are located only on the surrounding islands, not on the mainland ice sheet; ice sheet models include some of the larger islands, so there is some overlap in area, but the effect of this is estimated to be small (see 'Comparison with IPCC assessments' for an estimate of this and other limitations).

All projections are calculated as annual global mean sea level contributions since 2015, converting mass (for the glaciers) or mass above flotation (for the ice sheets) to sea level contribution using 362.5 Gt per mm SLE.

Global climate model simulations

We use projections of annual global mean surface air temperature change since 2015 from the CMIP5 and CMIP6 global climate models used to drive the ice sheet and glacier models to build the emulator. If multiple realisations (different initial conditions) for a model were available, we use the mean of these. Data from 1850-2100 were downloaded from the JASMIN/CEDA archive and ESGF on the 7th November 2019 and 4th December 2019; the CMIP6 snapshot was updated 28th-29th July 2020.

Emulation

An emulator is a fast statistical approximation of a computationally expensive simulator. This can be used to predict the simulator response at untried input values – to explore the uncertain input space far more thoroughly – for sensitivity analysis, to adjust the chosen inputs, and to estimate probability distributions. We construct statistical models of the simulated ice sheet and glacier sea level contribution as a function of the global mean surface air temperature of the driving climate models – and also different representations of the ice sheet-ocean interface – to make predictions under new emissions scenarios that incorporate these uncertainties, as well as those arising from the different structures of the climate and ice sheet models (and the emulators themselves).

Typically emulation is performed for one model at a time²⁴, but here we emulate each multi-model ensemble all at once. This is made possible by the systematic design of the ISMIP6 and GlacierMIP projects, which explore uncertainties in global climate change and three ice-ocean parameters simultaneously, and by our approach of applying emulation to multiple models rather than (as is usual) one. The three ice-ocean parameters control: (1) how much Greenland marine-terminating glaciers retreat (κ) with increasing local ocean temperatures and meltwater runoff; (2) how much Antarctic ice-shelf basal melting (γ) increases with increasing local ocean temperature; and (3) an on/off scenario of Antarctic ice shelf collapse (C), which can increase glacier flow into the ocean when atmospheric temperatures rise⁴⁶.

We predict the 23 land ice regions separately – the Greenland ice sheet, the West and East Antarctic ice sheets and Antarctic Peninsula, and 19 glacier regions – so the spatial distribution of meltwater can be used in regional sea level projections.

We choose and evaluate emulator structures using the year 2100 (Extended Data Table 2; Extended Data Figures 1 and 2). Global mean surface air temperature projections are taken from the FaIR simple climate model³⁰, because it can explore uncertainties more thoroughly than the relatively small CMIP6 ensemble of (computationally expensive) general circulation models. We use the same global mean temperature value across all land ice sources for each individual estimate: in other words, we include any co-dependence arising from global temperature. Full details are described in the following sections.

Global mean surface air temperature

Previous sea level emulation studies^{25,26,28,29} have typically used global mean temperature as the main input, rather than regional climate variables. We follow this approach for several reasons: to include correlation of land ice regions induced by global climate change (i.e. no need to assume/estimate their correlations, or to treat them as independent), and to have a larger sample of climate change projections. Using regional climate variables would improve the signal to noise for the emulator, but would restrict us to using computationally expensive general circulation models from CMIP5/6, for which there only a few tens of models. The simple climate model FaIR can be used to explore uncertainties in each scenario thoroughly, using the latest assessments of equilibrium climate sensitivity.

Global mean temperature is the only regressor for the glacier regions. For the ice sheets, there are additional terms derived from the ISMIP6 parameterisations of ice-ocean interactions.

Ice sheet model parameters

The Greenland glacier retreat parameter κ (Fig. 3a; units $\text{km} (\text{m}^3 \text{s}^{-1})^{-0.4} \text{°C}^{-1}$) is a scaling coefficient relating marine-terminating glacier retreat to ocean temperatures and meltwater runoff^{10,11}, where larger negative values indicate greater retreat of the glacier terminus in response to warming. This is a continuous variable, but most simulations use one of three values: the default, which is the median of the distribution in the parameterisation¹¹, $\kappa_{50} = -0.17$, and the quartiles $\kappa_{25} = -0.37$ and $\kappa_{75} = -0.06$. One model uses 5th and 95th percentile values, $\kappa_5 = -0.9705$ and $\kappa_{95} = 0.0079$. For ice sheet models that did not use this parameterisation ($N = 29$ simulations)¹⁴, we assign the mean value from the other simulations

to minimise the impact on the emulator ($\kappa = -0.2073$). One of these models (BISICLES) also ran 'high' and 'low' retreat experiments by doubling and halving the ocean thermal forcing, to which we assign the κ_{25} and κ_{75} values.

The Antarctic sub-shelf basal melt parameter γ (Fig. 3b; units m a^{-1}) is the 'ocean heat exchange velocity' scaling coefficient relating sub-shelf basal melting to ocean temperatures^{12,13}. Two alternative distributions for γ were derived in the parameterisation¹³: the first from mean Antarctic melt rates, and the second from the 10 highest observations of melt rate at the grounding line of Pine Island Glacier, where melt rates are currently highest. The values of γ estimated from Pine Island Glacier are an order of magnitude larger, and the two distributions do not overlap. This is a continuous variable, but most simulations use one of three values: the default, which is the median of the Mean Antarctic distribution, $\text{MeanAnt}_{50} = 14477$, and the 5th and 95th percentiles, $\text{MeanAnt}_5 = 9619$ and $\text{MeanAnt}_{95} = 21005$. Further simulations used the same percentiles from the Pine Island Glacier distribution: $\text{PIG}_{50} = 159188$, $\text{PIG}_5 = 86984$ and $\text{PIG}_{95} = 471264$. Some models¹⁵ used an alternative variant of the parameterisation in which only local ocean temperatures were used, rather than a combination of local and regional, which uses a different tuning for γ . However, the values used are also the 50 [5, 95]th percentiles of those distributions, so we consider them equivalent. For ice sheet models that did not use this parameterisation ($N = 62$ simulations), we again assign the ensemble mean value ($\gamma = 59317$).

The Antarctic ice shelf collapse parameter C is a switch that indicates whether a scenario of ice shelf collapse was used, which can lead to glacier speed-up. A timeline of collapses was derived according to the presence of surface meltwater on ice shelves above a threshold (725 mm a^{-1}) for 10 years, estimated from surface air temperature projections⁴⁶ in the global climate model driving the ice sheet model (mostly CCSM4). This method does not predict whether meltwater may be efficiently drained from the surface for a given ice shelf⁴⁷, thus avoiding collapse. We use values of 1 or 0 indicating whether the scenario is implemented or not.

Gaussian Process emulation

Gaussian Process emulation⁴⁸ is non-parametric, treating the simulator as an unknown mathematical function of its inputs. We use the R package RobustGaSP⁴⁹ for its numerically

robust parameter estimation⁵⁰. There are 23 emulators for the 2100 projections (Greenland ice sheet, three Antarctic ice sheet regions, and 19 glacier regions) and 1955 emulators for the full land ice time series (23 regions for each year from 2016 to 2100). An alternative to predicting each year separately would be to model the temporal correlation explicitly, but we prefer to use the simpler method, with fewer judgments, and allow temporal correlation to emerge.

Nugget

We use a ‘nugget’ term to incorporate simulations from each multi-model ensemble. The nugget is usually zero for deterministic models – the emulator predicts each simulation in the ensemble exactly, i.e. the regression curve goes through all points – or a very small value, to improve numerical stability or other properties^{22,23}. Here we allow the emulator to estimate the nugget, and treat each multi-model ensemble as a set of outputs from a single stochastic simulator or set of noisy observations. This approach has previously been used for emulating stochastic simulators⁵¹ and for emulating climate models accounting for internal variability, other inert inputs (uncertainties not explicitly modelled in the emulator), and approximations of the model outputs⁵²⁻⁵⁷. Our method is similar to the use of ‘emergent constraints’ for climate models^{44,58}, seeking relationships between past and future simulations across multi-model ensembles to constrain them with observations, but here the predictors are inputs to the models rather than their outputs for the past.

This approach does not require the simulations to be normally distributed but does assume they are independent, which has been a long-standing difficulty of interpreting multi-model climate ensembles. But with ice sheet models, although model names may be the same across groups, each one has a very different set up, including physics approximations, parameterisations, tuning, grid resolution, and – in particular – initialisation methods, which have been shown to produce very different results even for simulations produced by the same group^{6,7,14,15,59-61}. For glacier models, their structures are also vastly different, ranging from simple scaling parameterisations to dynamic physical models⁸. We test two approaches to account for any model dependence: a dummy variable (see below) and random effects (‘Antarctic cross-check model’).

Statistical model

Let y denote the simulated global mean sea level contribution for given region and year (in cm SLE), and \mathbf{x} the simulator inputs (see below). Following ref. [22], we write the simulator as a function $y = f(\mathbf{x})$, for which the Gaussian Process emulator is described by a mean function:

$$E[f(\mathbf{x})] = \mathbf{h}(\mathbf{x})^T \boldsymbol{\beta},$$

where $\mathbf{h}(\mathbf{x})$ is a vector of regression functions and $\boldsymbol{\beta}$ the corresponding regression coefficients, and a covariance function, with variance σ^2 and correlation function $c(\mathbf{x}, \mathbf{x}')$,

$$\text{Cov}[f(\mathbf{x}), f(\mathbf{x}')] = \sigma^2(c(\mathbf{x}, \mathbf{x}') + \nu \mathbf{I}),$$

where ν is the nugget term and \mathbf{I} the identity matrix. So the prior for $f(\mathbf{x})$ is:

$$p(f(\mathbf{x}) \mid \boldsymbol{\beta}, \sigma^2, \delta, \nu) \sim N(\mathbf{h}(\mathbf{x})^T \boldsymbol{\beta}, \sigma^2(c(\mathbf{x}, \mathbf{x}') + \nu \mathbf{I})),$$

where \mathbf{x} are whichever model inputs are used for a given region, δ are the correlation lengths of the covariance function, and $\sigma^2\nu$ is the variability not explained by the inputs. Parameters $(\boldsymbol{\beta}, \sigma^2, \delta, \nu)$ are estimated from the simulation data.

The inputs \mathbf{x} used in the regression functions are global mean temperature change, T , and, for the ice sheets, the ice-ocean parameter values (κ for Greenland; γ , C for Antarctica), plus a dummy variable denoting whether Greenland models used the retreat parameterisation. These are discussed in the next section. All inputs are rescaled to have zero mean and unit variance.

Mean functions

The Gaussian Process mean function describes the large-scale response of the simulator to its inputs, usually specified as a linear trend with the remainder described by a zero-mean Gaussian process.

For the glaciers, the linear regressor is simply global mean temperature in the same year (T).

For the ice sheets, the additional ice sheet model parameters are κ for Greenland, and γ and C

for Antarctica. We also try two types of dummy variable. The first is for the ice sheet and glacier model names, so these can be treated distinctly in the emulator, but this leads to clear overfitting (i.e. the model is too flexible in Figs. 1 and 2). The second represents whether an ice sheet model uses the ISMIP6 retreat or basal melt parameterisation, to absorb any misalignment between the imputed value and the effective value. Bayesian Information Criterion (BIC) from a stepwise model selection (testing up to first-order interactions) suggests this dummy variable is informative for Greenland, so we retain it (o , for open parameterisation), but not for the Antarctic regions. The stepwise model selection suggests we could reasonably include terms for the interaction between temperature and retreat for Greenland, temperature and basal melt for West Antarctica, and temperature and collapse for East Antarctica, but we choose not to, to avoid the risk of overfitting. The selection also shows that collapse strongly dominates the Antarctic Peninsula response, and is may not be needed for West Antarctica, but we retain all terms (i.e. T_i , γ_0 , C) because we otherwise find the covariance matrix is poorly conditioned. The resulting mean functions are $h_{\text{GrIS}}(\mathbf{x})_i \sim (T_i, k, o)$ for Greenland, $h_{\text{AIS}}(\mathbf{x})_i \sim (T_i, \gamma_0, C)$ for the Antarctic regions, and $h_{\text{Glaciers}}(\mathbf{x})_i \sim (T_i)$ for the glaciers, where $h \sim (a, b)$ means h is a linear function of a and b , and i is the index for the year.

Covariance functions

The covariance function describes the smoothness of the Gaussian Process. As in any statistical modelling, there is a trade-off between improving accuracy and over-fitting. We assess this using the usual leave-one-out procedure^{62,63}. We fit the emulator to all ensemble members but one, then predict the sea level contribution from this simulation; we repeat this for every combination, noting the emulator error (residual) and uncertainty for each prediction. We perform this for each of the 23 regional emulators for the year 2100 with five covariance functions of varying smoothness – Matérn(5/2), which is the default in RobustGaSP, Matérn (3/2), and three members of the power exponential family with high, medium and low exponent values ($\alpha = 1.9$, i.e. close to a squared exponential, the default value; $\alpha = 1.0$, exponential, and $\alpha = 0.1$, for which the covariance function has a small effect so the emulator approaches linear regression).

For 18 of the 19 glacier regions, we use the covariance function with the smallest standardised Euclidean distance between the emulator predictions and simulations

(standardised because, unlike simpler metrics such as root mean square error or mean absolute error, it does not penalise larger errors if the emulator uncertainty intervals are sufficiently large), as in ref [24]. For the Southern Andes (region 17), all covariance functions give identical distances, so we use the default for RobustGaSP. For the ice sheets, we use the covariance function that gives close to linear regression (power exponential, $\alpha = 0.1$), rather than the one with the minimum Euclidean distance, for various reasons. For Greenland, West Antarctica, and the Antarctic Peninsula, the minimum distance covariance functions (power exponential $\alpha = 1.0$ for Greenland; Matérn(3/2) for the Antarctic regions) result in overfitting for temperature (i.e. too much flexibility in Fig. 1). For East Antarctica, the minimum distance covariance functions (Matérn(5/2)) result in an incorrect sign prediction under the ice shelf collapse switch. Using the alternative covariance function solves all of these issues and does not increase the standardised Euclidean distance by much: 4% for the Peninsula, and 0.4-1% for the other three regions. The resulting covariance functions are given in Extended Data Table 2.

Evaluating the emulators

After selecting the covariance functions for each regional emulator at 2100, we evaluate the emulators further by plotting the emulator predictions against the simulations from the leave-one-out procedure, and the standardised residuals (the difference between the emulator prediction and the simulator, divided by the emulator standard deviation), and calculating the percentage of simulations falling within ± 2 s.d. (Extended Data Table 2 and Extended Data Figures 1 and 2). We would not expect exactly 95% of the simulations to fall within 2 s.d., in part because the predictions are not independent, but very low or high values would suggest emulator over- or under-confidence. The region with the lowest percentage of predictions within the uncertainty intervals is North Asia (region 10) with 89%, indicating slightly too small emulator uncertainty estimates, and the highest is 98% (Scandinavia: region 8), indicating the reverse.

Mean absolute errors for each emulator are given in Extended Data Table 2 and Extended Data Figures 1 and 2: for the ice sheet regions they are 0.28 cm (Peninsula), 1.4 cm (Greenland) and 1.5 cm (East Antarctica) and 2.0 cm (West Antarctica), and for the

individual glacier regions they range from 0.0020 cm to 0.87 cm (Antarctic periphery: region 19). Mean absolute standardised errors are all less than 0.006.

The emulator underestimates the three to four highest West and East Antarctic contributions by around 10-15 cm (Extended Data Figure 1b and 1c). The five highest of these are from the SICOPOLIS model, which has a much greater sensitivity to basal melting than other models (see main text, *Robustness checks* and Extended Data Figure 6), and use the highest value of this parameter ($\gamma = \text{PIG}_{95}$). These simulations are therefore extreme: 1% of the 344 simulations, and the 97.5th percentile value of the basal melt parameter. There are process-based reasons to expect that SICOPOLIS is an upper bound or overestimate (see main text). When the emulator is calibrated with this model alone, it does not underestimate its highest contributions (not shown). The resulting projections under the NDC scenario are shown in *Robustness checks* (test 4); the difference with the main projections may be interpreted as the maximum possible impact of this emulator underestimate, if SICOPOLIS were the sole realistic ice sheet model. These are lower than the 'risk-averse' projections, which are made with a subset of high sensitivity ice sheet models and other pessimistic assumptions (see main text).

We therefore consider the emulators to be adequate for the predictions of large-scale sea level contribution presented here.

Antarctic cross-check model

We perform a cross-check for the Antarctic ice sheet regions at 2100 using a linear mixed model, with the ice sheet model name included as a random effect to deal with any systematic uncertainty arising from dependence of ensemble members. This attributes some of the uncertainty in the response to the ice sheet model used, and this uncertainty can then be removed from the predicted PDF. We thus model the ensemble members as 'similar but not identical', using a mean function of temperature and ice sheet parameters, plus a structured error term which includes a systematic component according to the ice sheet model and a noise component to capture other sources of variability such as initialisation.

For the mean function (also linear), we use the logarithm of γ as a regressor, so it is always positive. Consequently we use the geometric mean as the missing value, rather than the arithmetic mean. We use a dummy variable to denote these models, as for Greenland in the GP emulator. The full global mean temperature change trajectories are used instead of only the total change at 2100. To increase the signal-to-noise ratio, the annual means are reduced to decadal means (2015–2029, 2030–2039, . . . , 2090–2100). There are thirteen distinct forcings, each one the product of a global climate model and a scenario, so we represent the forcing variables as twelve bisquare basis functions. These start as thirteen bisquare basis functions, each one centred at one of the thirteen forcings, but one is dropped because otherwise the model matrix becomes rank deficient when a constant is added. The one dropped is the one with the smallest mean Euclidean distance to the other twelve. We use bisquare kernels, where the standard deviation of each kernel is set to one tenth of the maximum Euclidean distance between all pairs of forcings, to cover the forcing space with non-zero values for the forcing regressors. We use the same distributions for temperature, basal melt and collapse as the main projections, and set the dummy variable to represent standard parameterisation models.

This emulator predicts 50 [5, 95]th percentiles for the West Antarctic sea level contribution at 2100 of 2 [-4, 8] cm SLE for SSP1-26 and 3 [-4, 10] cm SLE for SSP5-85, which are very similar to the GP emulator predictions of 2 [-5, 10] cm SLE and 3 [-4, 11] cm SLE. We test the effect of changing the kernel standard deviation to one twelfth or one fourteenth of the maximum Euclidean distance; the largest change is a 2 cm decrease in the 95th percentile under SSP5-85. For East Antarctica, the emulator with random effects predicts 2 [-3, 6] cm SLE for both scenarios; the GP emulator predicts a small scenario-dependence, 2 [-4, 7] cm SLE for the low emissions scenario and 0 [-5, 6] cm SLE for the high. For the Antarctic Peninsula, the random effects predictions are 0 [-1, 2] cm SLE for both scenarios, and the GP are the same. These similarities give us confidence that model dependence is not substantially affecting our projections – i.e. that differences in model structure, resolution, calibration and initialisation dominate over the similarities – although it would be worth investigating this in more detail.

Sea level projections

We use probability distributions for global temperature and the ice sheet model parameters as inputs to each emulator to make the projections.

Global mean temperature projections

We use projections of global annual mean surface air temperature change since 2015 from the FaIR (Finite amplitude Impulse Response) simple climate model for the main projections. We take the 500-member ensemble from reference [30]: SSP1-19, SSP1-26, SSP3-70, SSP5-85 and a scenario estimated for the 2019 Nationally Determined Contributions. We also use projections for SSP-245 generated with the same ensemble.

Ice sheet model parameter distributions

For Greenland, we sample from a kernel density estimate of the original k distribution ($N = 191$) with the same bandwidth used in deriving the parameterisation^{10,11} (0.0703652) (Fig. 1b). The dummy variable is always set to represent the standard ISMIP6 parameterisation.

For Antarctica, we combine the Mean Antarctic and Pine Island Glacier γ distributions ($N = 10,000$ each), and sample from a kernel density estimate using three times the automatic bandwidth (Silverman's 'rule of thumb'⁶⁴) to merge and smooth them into a near-unimodal distribution that we truncate at zero (Fig. 1c). For the collapse switch C , we sample randomly from 0 or 1 with equal probability (8% of the ISMIP6 simulations have ice shelf collapse). The ice shelf collapse scenario does not include the possibility of surface meltwater draining efficiently from some ice shelves under certain conditions, thereby avoiding collapse, so we feel this is a reasonable judgement.

Sampling

For the 2100 projections, we sample from the FaIR ensemble ($N=500$) with replacement ($N = 5000$ for main and risk-averse projections; $N = 1000$ for robustness and sensitivity tests). For the full time series, we use the 500 FaIR projections directly without resampling. We make one set of emulator predictions (23 regions) for each temperature value in a given year, randomly sampling the relevant ice-ocean parameters (k , γ_0 , C) once for each FaIR ensemble member.

We integrate over the uncertain inputs (temperature in a given year, and ice-ocean parameters) to obtain the final probability density functions (PDFs). Each regional emulator predicts a Student-t distribution for a given set of these input values, defined by a mean and standard deviation; we approximate this with a normal distribution, as in refs [55, 57], which is accurate enough for this application. We use different integration methods for the 23 individual regional PDFs compared with the regional sums (Antarctica, global glaciers, and land ice total). For the individual regional estimates, we use deterministic numerical integration (the midpoint rule: we sum the Gaussian distributions for each emulator prediction, then normalise). For regional sums we must use Monte Carlo sampling, because the three ice sources (Greenland, Antarctica and glaciers) have different parameters, and we also desire traceability of predictions to input values within a given ice source. We sample once from the Gaussian distribution for each emulator prediction, then sum the regional samples for a given temperature to estimate the PDF, smoothing with kernel density estimation for figures (again using Silverman's 'rule of thumb'⁶⁴ for the bandwidth). Sampling is a more noisy method of integration than deterministic methods, so the PDFs for regional sums are less smooth than those for individual regions.

Glacier maximum cap

We apply a cap to the glacier projections using estimates of their maximum sea level contribution³¹. Glacier model projections often exceed this cap in some regions, if near or total loss is projected under high emissions, either because they report changes in total mass, not mass above flotation, or because of errors in initial mass⁸, or both. We restrict values to the maximum in the emulator mean predictions and then the PDFs (the latter exceeding the cap due to emulator uncertainty).

Time series smoothing

Interannual variability arises in the time series due to sampling the emulator uncertainty for each annual regional prediction. We apply a five year running mean in Fig. 3d to visualise the expected smoothness of sea level contributions; projections provided in the Supplementary Information are unsmoothed.

Comparison with IPCC assessments

The ice sheet projections are made relative to control simulations with a constant recent climate. This control includes both the model drift and, depending on the initialisation method, any background contribution arising from forcing before 2015. This background contribution should be added to the ice sheet projections, but is difficult to quantify. Five year mean rates of sea level contribution since 1992/3 range from 0.1-0.8 mm/yr for the Greenland ice sheet⁶⁵ and 0.1-0.6 mm/yr for Antarctica⁶⁶, but they would decrease in the absence of forcing after 2014. Modelling work to quantify the background contribution from Greenland⁶⁷ suggests a contribution of 0.6 ± 0.2 cm SLE by 2100. Estimates made for this study range from 0.3-0.8 cm under a range of retreat parameter values, $\kappa_{75} - \kappa_{25}$ (IMAU/IMAUICE1: 0.3-0.4 cm; CISM variant similar to NCAR/CISM: 0.4-0.8 cm). For Antarctica, the dynamic commitment has been estimated to be 2 cm SLE at 2100 for the Amunden Sea Embayment region of West Antarctica, where most mass loss is currently occurring⁶⁸. Part of these trends may still be due to residual model drift. The committed contribution could therefore add up to ~ 1 cm/century to our Greenland projections and ~ 2 cm/century to the Antarctic.

The Antarctic ice sheet models include some of the larger islands that are also included in region 19, potentially leading to double-counting. However, median projections for region 19 range from 1-2 cm under different emissions scenarios, and the ice sheet models are much lower resolution (i.e. the glaciers are likely less responsive), so the effect is expected to be of order 0.5-1 cm SLE or less.

We average our projections over the 86 years and compare them with the average IPCC AR5²⁵ and SROCC¹ projections over 95 years (the midpoints of 1986-2005 to 2081-2100) as rates of cm SLE per century. For the glaciers, we project 8 cm/century SLE for SSP1-26 and 16 cm/century for SSP5-85 excluding the Antarctic peripheral glaciers (region 19: 1 cm and 2 cm, respectively), compared with 10 cm for RCP2.6 and 17 cm for RCP8.5 in AR5. For the Greenland ice sheet, we project 4 cm/century SLE for SSP1-26 and 11 cm for SSP5-85, compared with 6 cm for RCP2.6 and 13 cm for RCP8.5 in AR5. For Antarctica, we project 5 cm/century SLE for both scenarios; the AR5 projections are 5 cm/century SLE for RCP2.6 and 4 cm for RCP8.5, while those for SROCC are 4 cm/century SLE for RCP2.6 and 11 cm

for RCP8.5. The difference between scenarios for Antarctica in AR5 arises only from additional accumulation, because the dynamic contributions are assumed to be the same.

Glacier projections could be overestimated because meltwater routing to the ocean is not accounted for (not all volume lost from the glaciers reaches the oceans), or underestimated because only one glacier model includes ice-water interactions (i.e. frontal ablation of marine- and lake-terminating glaciers). For the latter, we compare mean projections for the GloGEM model to the emulator for RCP8.5/SSP5-85 and RCP4.5/SSP2-45 for key regions, and find they are larger by less than 1 cm for Alaska and Russian Arctic (regions 1 and 9), by less than 0.5 cm for Svalbard (7) and Arctic Canada South (4), and smaller than the emulator for Arctic Canada North (3). All are within the emulator 95th percentile estimates. We may slightly underestimate uncertainty in the global glacier total due to correlated errors across models⁸ by emulating the regions independently, though there are compensating advantages (more accurate emulation; spatial pattern of meltwater); a similar argument applies to Antarctica.

Sensitivity tests

We perform a number of checks to test the sensitivity of the ice sheet projections to changes in the chosen inputs, predominantly the input distributions, but also the dataset in the final test (see Extended Data Table 3 and refs [25, 26, 30, 34, 39]). All results are shown for the SSP5-85 scenario in Extended Data Figure 4 under the index given (where 1 is the main projection); numerical values in the text refer to changes in the median and [5, 95th] percentile estimates for the ice sheet under this scenario unless otherwise stated.

Robustness checks

We perform a number of checks to test robustness of the ice sheet projections to changes in the simulation dataset (see Extended Data Table 4 and refs [14, 16, 24, 66]). Results are shown for the NDCs scenario in Extended Data Figure 5 under the test index given (where 1 is the main projection); numerical values in the text refer to changes in the median and [5, 95th] percentile estimates under this scenario unless otherwise stated. The full datasets are 256 simulations for Greenland and 344 simulations for Antarctica.

Parameter interactions

Retreat and basal melt vs temperature

Ice sheet projection uncertainties are constant across scenarios. However, tests with three ice sheet models show that the range of projections from high to low values of the retreat parameter ($\kappa_{95} - \kappa_5$) and basal melt parameter ($\text{PIG}_{95} - \text{MeanAnt}_{50}$) is consistently smaller under RCP2.6 than RCP8.5, so the emulator uncertainty should be smaller at lower temperatures. The ratios of ranges, RCP2.6/RCP8.5, for each group/model + GCM are:

Greenland

- $\text{IMAU/IMAUICE} + \text{MIROC5} = 1.4097/8.3069 = 0.17$
- $\text{IMAU/IMAUICE} + \text{CNRM-CM6-1} = 2.4813/9.7187 = 0.26$

West Antarctica

- $\text{JPL1/ISSM} + \text{NorESM1-M} = 0.40$
- $\text{CPOM/BISICLES} + \text{NorESM1-M} = 0.57$

East Antarctica

- $\text{JPL1/ISSM} + \text{NorESM1-M} = 0.73$
- $\text{CPOM/BISICLES} + \text{NorESM1-M} = 0.32$

The emulator does not have sufficient data from lower emissions scenarios to reduce the variance, particularly for Greenland. If other ice sheet models respond the same way as the above, then adding more simulations may reduce the uncertainty for low SSPs.

Ice shelf collapse vs basal melt

The contribution due to ice shelf collapse does not increase with higher values of the basal melt parameter in the models JPL1/ISSM and CPOM/BISICLES (0.1 cm difference for the Peninsula in BISICLES; all other regional differences for both models ≤ 0.02 cm).

Code availability

R code and input data are available at <https://github.com/tamsinedwards/emulandice>. Each simulation in the sea level projections file has a label in the 'publication' column for the reference (Goelzer2020, Seroussi2020, Nowicki2020 or Marzeion2020), or 'New' if previously unpublished.

Data availability

All global climate, simple climate, ice sheet and glacier model data used as inputs to this study are provided with the code as described above. Main and risk-averse projections from the analysis are provided in the Supplementary Information as annual quantiles for each of the 23 regions, and the Antarctic, glacier and land ice sums.

Author information

The authors declare no competing financial or non-financial interests. Correspondence and requests for materials should be addressed to T.L.E. (tamsin.edwards@kcl.ac.uk). Reprints and permissions information is available at www.nature.com/reprints.

Methods References

46. Trusel, L. D. *et al.* Divergent trajectories of Antarctic surface melt under two twenty-first-century climate scenarios. *Nature Geoscience* 8, 927–932 (2015).
47. Bell, R. E. *et al.* Antarctic ice shelf potentially stabilized by export of meltwater in surface river. *Nature* **544**, 344–348 (2017).
48. O'Hagan, A. Bayesian analysis of computer code outputs: A tutorial. *Reliability Engineering and System Safety* **91**, 1290–1300 (2006).
49. Gu, M. *et al.*, RobustGaSP: Robust Gaussian Stochastic Process Emulation in R, The R Journal (2019) 11:1, pages 112–136.
50. Gu, M., X. Wang and J.O. Berger (2018), Robust Gaussian stochastic process emulation, *Annals of Statistics*, 46(6A), 3038–3066.
51. van Beers, W. C. M. & Kleijnen, J. P. C. Kriging for interpolation in random simulation. *Journal of the Operational Research Society* 54, 255–262 (2017).
52. Salter, J. M. & Williamson, D. A comparison of statistical emulation methodologies for multi-wave calibration of environmental models. *Environmetrics* 27, 507–523 (2016).
53. Williamson, D. & Blaker, A. T. Evolving Bayesian Emulators for Structured Chaotic Time Series, with Application to Large Climate Models. *SIAM/ASA J. Uncertainty Quantification* 2, 1–28 (2014).
54. Williamson, D., Blaker, A., Hampton, C. & Salter, J. Identifying and removing structural biases in climate models with history matching. *Climate Dynamics* **45**, 1299–1324 (2014).
55. Araya-Melo, P. A., Crucifix, M. & Bounceur, N. Global sensitivity analysis of the Indian monsoon during the Pleistocene. *Climate of the Past* **11**, 45–61 (2015).
56. Bounceur, N., Crucifix, M. & Wilkinson, R. D. Global sensitivity analysis of the climate–vegetation system to astronomical forcing: an emulator-based approach. *Earth Syst. Dynam.* **6**, 205–224 (2015).
57. Lord, N. S. *et al.* Emulation of long-term changes in global climate: application to the late Pliocene and future. *Climate of the Past* **13**, 1539–1571 (2017).
58. Bowman, K. W. *et al.* (2018). A hierarchical statistical framework for emergent constraints: Application to snow-albedo feedback. *Geophysical Research Letters*, 45, 13,050–13,059. <https://doi.org/10.1029/2018GL080082>
59. Nowicki, S. *et al.* Insights into spatial sensitivities of ice mass response to environmental change from the SeaRISE ice sheet modeling project I: Antarctica. *J Geophys Res-Earth* **118**, 1002–1024 (2013).
60. Nowicki, S. *et al.* Insights into spatial sensitivities of ice mass response to environmental change from the SeaRISE ice sheet modeling project II: Greenland. *J Geophys Res-Earth* **118**, 1025–1044 (2013).
61. Saito, F., Abe-Ouchi, A., Takahashi, K. & Blatter, H. SeaRISE experiments revisited: potential sources of spread in multi-model projections of the Greenland ice sheet. *The Cryosphere* **10**, 43–63 (2016).
62. Rougier, J., Sexton, D. M. H., Murphy, J. M. & Stainforth, D. A. Analyzing the Climate Sensitivity of the HadSM3 Climate Model Using Ensembles from Different but Related Experiments. *J Climate* **22**, 3540–3557 (2009).
63. Bastos, L. S. & O'Hagan, A. Diagnostics for Gaussian Process Emulators. *Technometrics* **51**, 425–438 (2009).
64. Silverman, B. W. (1986). *Density Estimation*. London: Chapman and Hall.

65. The IMBIE team. Mass balance of the Greenland Ice Sheet from 1992 to 2018. *Nature* 1–25 (2019). doi:10.1038/s41586-019-1855-2
66. The IMBIE team. Mass balance of the Antarctic Ice Sheet from 1992 to 2017. *Nature* **558**, 219–222 (2018).
67. Price, S. F., Payne, A. J., Howat, I. M., and Smith, B. E.: Committed sea-level rise for the next century from Greenland ice sheet dynamics during the past decade, *P. Natl. Acad. Sci. USA*, 108, 8978–8983, 2011.
68. Alevropoulos-Borrill, A. V., Nias, I. J., Payne, A. J., Golledge, N. R. & Bingham, R. J. Ocean-forced evolution of the Amundsen Sea catchment, West Antarctica, by 2100. *The Cryosphere* **14**, 1245–1258 (2020).

Extended Data

Extended Data Table 1. The additional 22 Greenland and 37 Antarctic ice sheet model experiments not previously described elsewhere. Retreat parameter values κ_5 and κ_{95} are the 5th and 95th percentile values of the retreat (κ) distribution; basal melt parameter values $\text{MeanAnt}_{[5, 50, 95]}$ and $\text{PIG}_{[5, 50, 95]}$ are the 5th, 50th and 95th percentile values of the Mean Antarctic and Pine Island Glacier basal melt (γ) distributions (see Methods).

Extended Data Table 2. Emulator structure and validation. Emulator covariance functions, and the results of the leave-one-out procedure for each: the percentage of simulations that fall within the emulator 95% uncertainty intervals, and the mean absolute error.

Extended Data Figure 1. Emulator leave-one-out validation for ice sheets and 8 glacier regions. Left of each subpanel: Emulator predictions versus simulations for each regional sea level contribution in the year 2100, with percentage of predictions falling outside ± 2 emulator standard deviations and mean absolute error in cm SLE. Right of each subpanel: standardised residuals (emulated minus simulated, divided by emulator standard deviation). Predictions falling outside ± 2 emulator standard deviations are shown in orange.

Extended Data Figure 2. Emulator leave-one-out validation for 11 glacier regions. As for Extended Data Figure 1, but for the remaining glacier emulators.

Extended Data Figure 3. Temperature projections for 2015-2100 from FaIR and CMIP6 ensembles. Global surface air temperature projections under different greenhouse gas scenarios (see main text) from the (a) FaIR simple climate model ensemble ($N = 5000$; same as Figure 3a) and (b) CMIP6 global climate model ensemble ($N \sim 30$ models per scenario: see Methods) sampled with a kernel density estimate ($N = 1000$).

Extended Data Table 3. Sensitivity tests. Tests of the sensitivity of the ice sheet projections to changes in the chosen inputs. The test index, name, description and impact are detailed. Numerical values refer to changes in the median and [5th, 95th] percentile estimates for the ice sheet under SSP5-85, unless otherwise stated; results for this scenario are shown in Extended Data Figure 4.

Extended Data Figure 4. Sensitivity of ice sheet projections at 2100 under SSP5-85 to uncertain inputs. a, Greenland. b, West Antarctica. c, East Antarctica. d, Antarctic Peninsula. Indices refer to test (see Extended Data Table 3). Box and whiskers show [5, 25, 50, 75, 95]th percentiles. 1: Default; 2: CMIP6 global climate model ensemble projections of global mean surface air temperature, instead of FaIR simple climate model; 3: fixed global mean surface air temperature; 4: fixed glacier retreat (Greenland) or

basal melt (Antarctica) parameter. Antarctic regions only: basal melt parameter has 5: 'Mean Antarctic' distribution; 6: 'Pine Island Glacier' distribution; 7: uniform, high distribution; 8: uniform, very high distribution. Ice shelf collapse scenario: 9: off and 10: on. 11: Risk-averse projections using the high 'Pine Island Glacier' distribution for basal melt (test 6), ice shelf collapse on (test 10), and the ice sheet and climate models that give the highest sea level contributions (Extended Data Figure 5: test 6, 7).

Extended Data Table 4. Robustness checks. Checks performed to test the robustness of the ice sheet projections to changes in the simulation dataset. The test index, name, description and impact are detailed. Numerical values refer to changes in the median and [5th, 95th] percentile estimates for the ice sheet under the NDCs scenario, unless otherwise stated; results for this scenario are shown in Extended Data Figure 5.

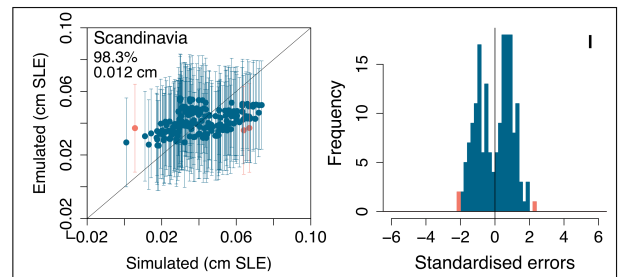
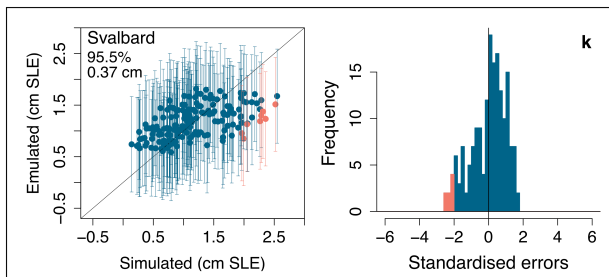
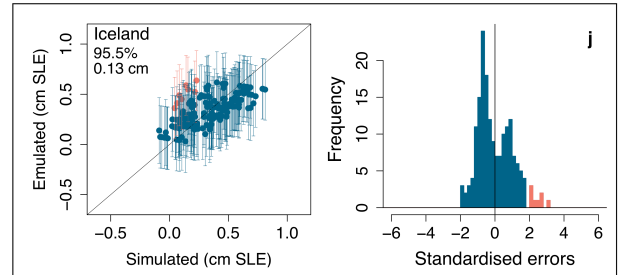
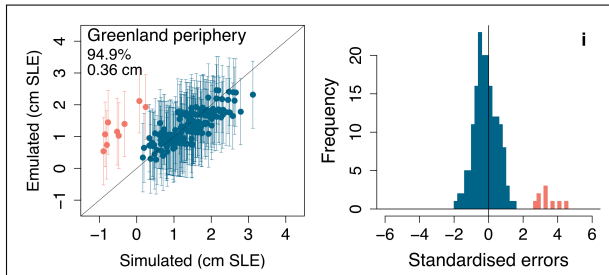
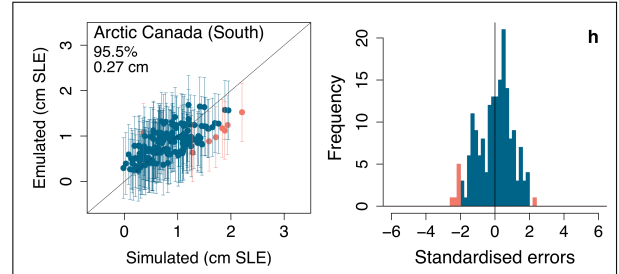
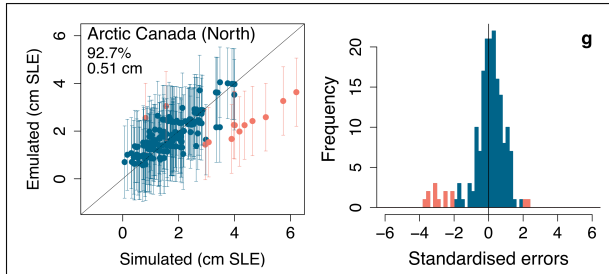
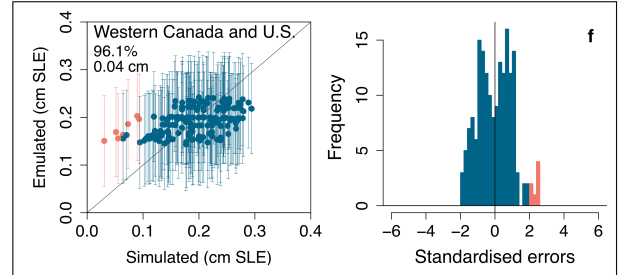
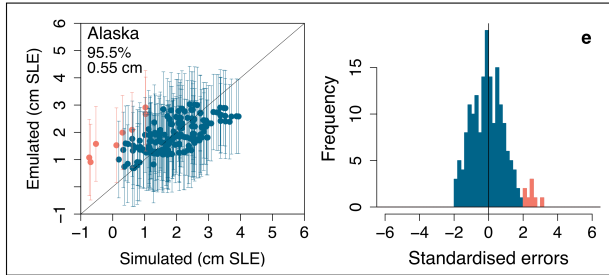
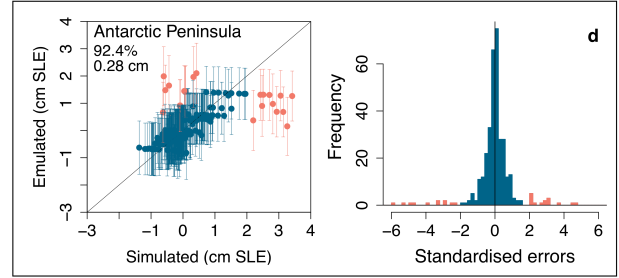
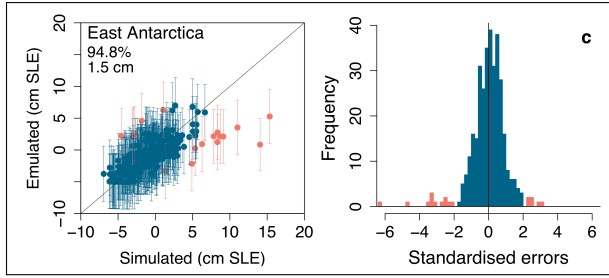
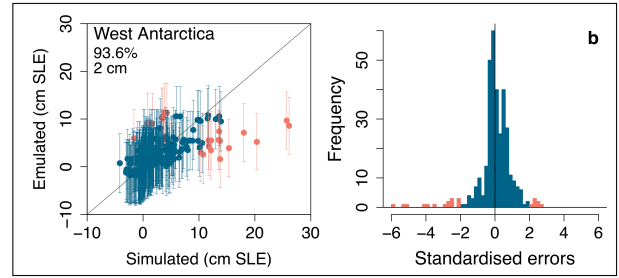
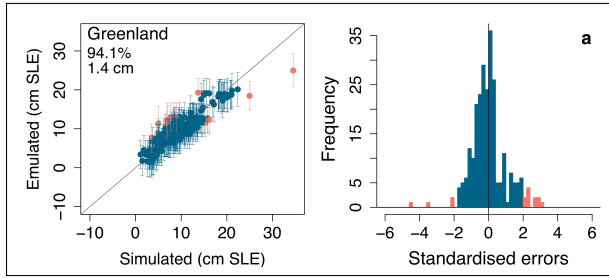
Extended Data Figure 5. Robustness of ice sheet projections under Nationally Determined Contributions to ice sheet/climate model simulation selection and treatment. a, Greenland. b, West Antarctica. c, East Antarctica. d, Antarctic Peninsula. Indices refer to test (see Extended Data Table 4). Box and whiskers show [5, 25, 50, 75, 95]th percentiles. 1: Default; 2: Higher resolution ice sheet models; 3: Ice sheet models with the most complete sampling of uncertainties (10 models for Greenland, 4 for Antarctica); 4: Single ice sheet model with the most complete sampling of uncertainties and (coincidentally) high sensitivity to retreat or basal melting parameter. Antarctic regions only; 5: Alternative single ice sheet model with nearly as complete sampling but low sensitivity to basal melt parameter. 6: Ice sheet models with the highest sensitivity to basal melt parameter; 7: Climate models that lead to highest sea level contributions. 8: Ice sheet models with 2015-2020 mass change in the range 0-0.6 cm. 9: Only ice sheet models that use the standard ISMIP melt parameterisations. 10: Higher basal melt value assigned to ice sheet models that do not use the standard ISMIP6 melt parameterisations.

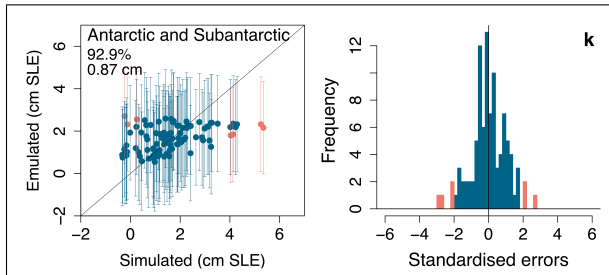
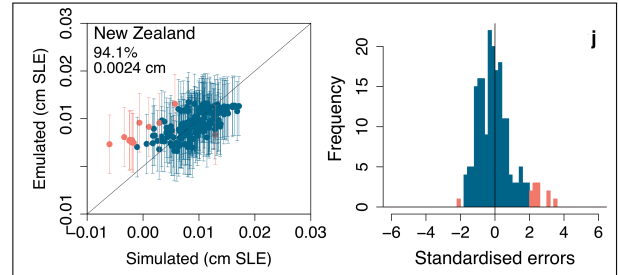
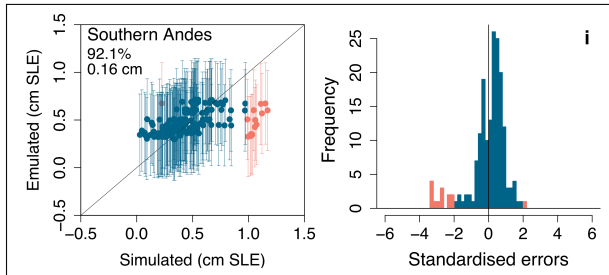
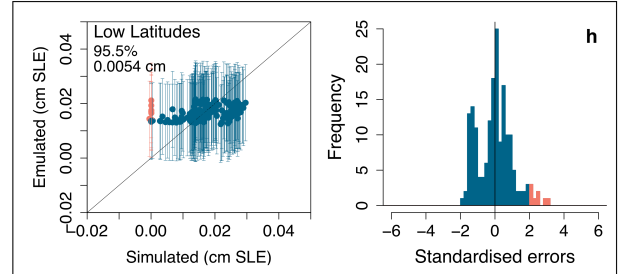
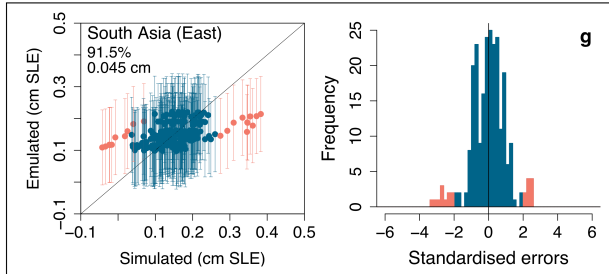
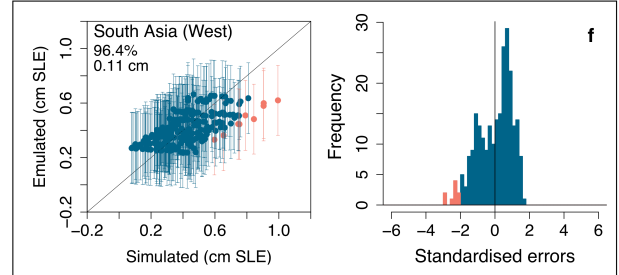
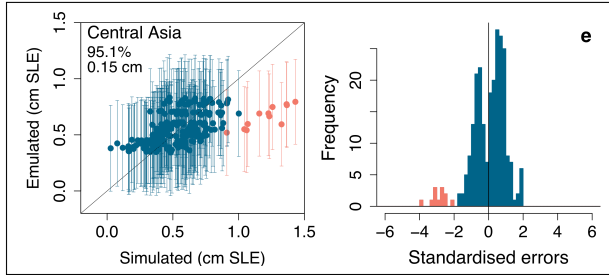
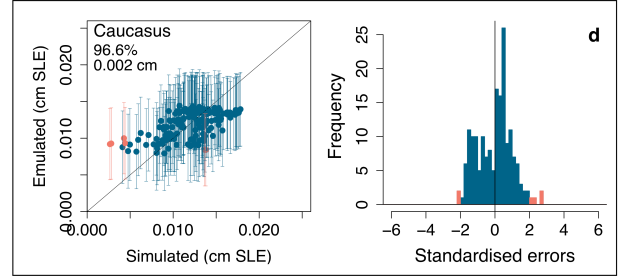
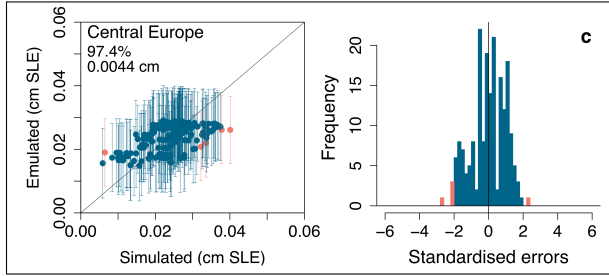
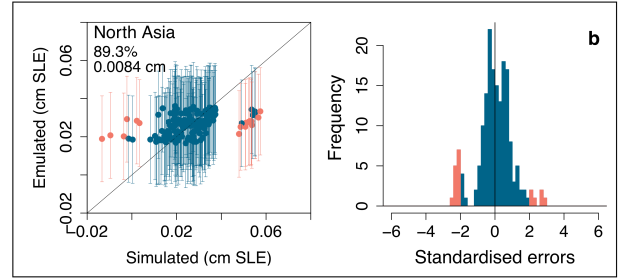
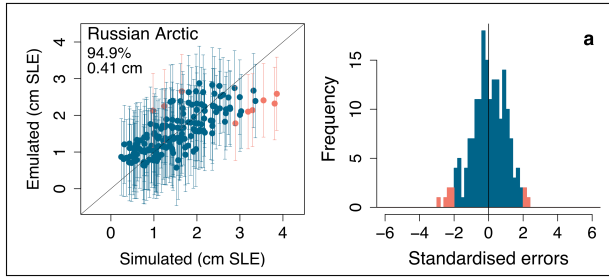
Extended Data Figure 6. Sensitivity to basal melting by Antarctic ice sheet and climate model. Vertical lines show ice sheet models that do not use the ISMIP6 basal melt parameterisation, and the basal melt value they are assigned. Ice sheet models includes the high and low sensitivity models in Extended Data Figure 5: test 4 (ILTS_PIK/SICOPOLIS) and test 5 (LSCE/GRISLI).

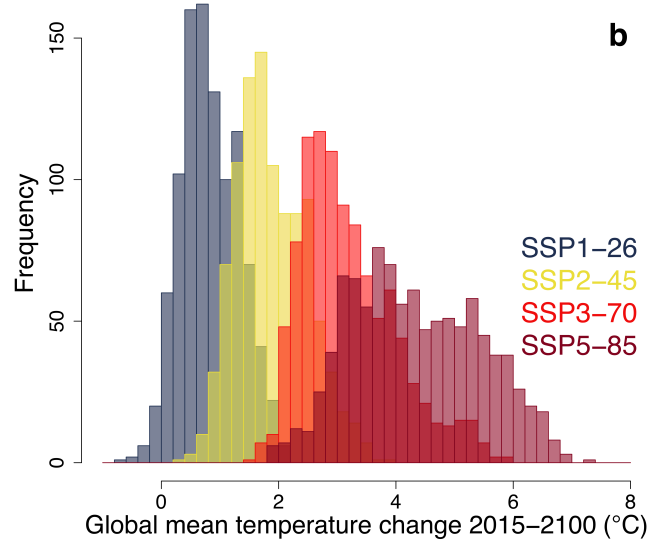
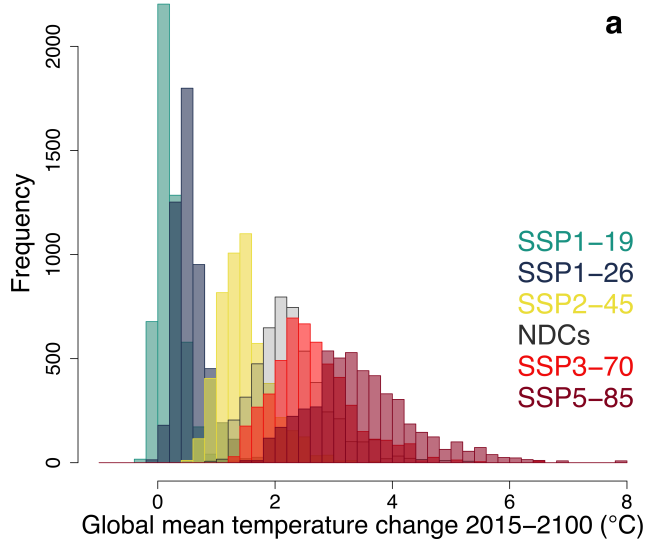
Extended Data Figure 7. Effect of Antarctic ice shelf collapse by climate model. Additional sea level contribution at 2100 when using ice shelf collapse for six climate models, ordered by maximum impact on the Peninsula contribution. (a) West and (b) East Antarctica, and (c) Peninsula.

Additional Greenland experiments				
Experiment name	Scenario	Climate model	Retreat parameter	
expe01	RCP8.5	NorESM1-M	K ₉₅	
expe02	RCP8.5	NorESM1-M	K ₅	
expe03	RCP8.5	HadGEM2-ES	K ₉₅	
expe04	RCP8.5	HadGEM2-ES	K ₅	
expe05	RCP2.6	MIROC5	K ₉₅	
expe06	RCP2.6	MIROC5	K ₅	
expe07	RCP8.5	IPSL-CM5A-MR	K ₉₅	
expe08	RCP8.5	IPSL-CM5A-MR	K ₅	
expe09	RCP8.5	CSIRO-Mk3-6-0	K ₉₅	
expe10	RCP8.5	CSIRO-Mk3-6-0	K ₅	
expe11	RCP8.5	ACCESS1-3	K ₉₅	
expe12	RCP8.5	ACCESS1-3	K ₅	
expe13	SSP5-85	CNRM-CM6-1	K ₉₅	
expe14	SSP5-85	CNRM-CM6-1	K ₅	
expe15	SSP1-26	CNRM-CM6-1	K ₉₅	
expe16	SSP1-26	CNRM-CM6-1	K ₅	
expe17	SSP5-85	UKESM1-0-LL	K ₉₅	
expe18	SSP5-85	UKESM1-0-LL	K ₅	
expe21	SSP5-85	CNRM-ESM2-1	K ₉₅	
expe22	SSP5-85	CNRM-ESM2-1	K ₅	
expe23	RCP8.5	MIROC5	K ₉₅	
expe24	RCP8.5	MIROC5	K ₅	
Additional Antarctic experiments				
Experiment name	Scenario	Climate model	Basal melt (γ ₀)	Ice shelf collapse (C)
Basal melt parameter values				
expD1	RCP8.5	MIROC-ESM-CHEM	MeanAnt ₉₅	Off
expD2	RCP8.5	MIROC-ESM-CHEM	MeanAnt ₅	Off
expD3	RCP2.6	NorESM1-M	MeanAnt ₉₅	Off
expD4	RCP2.6	NorESM1-M	MeanAnt ₅	Off
expD5	RCP8.5	CCSM4	MeanAnt ₉₅	Off
expD6	RCP8.5	CCSM4	MeanAnt ₅	Off
expD7	RCP8.5	HadGEM2-ES	MeanAnt ₉₅	Off
expD8	RCP8.5	HadGEM2-ES	MeanAnt ₅	Off
expD9	RCP8.5	CSIRO-Mk3-6-0	MeanAnt ₉₅	Off
expD10	RCP8.5	CSIRO-Mk3-6-0	MeanAnt ₅	Off
expD11	RCP8.5	IPSL-CM5A-MR	MeanAnt ₉₅	Off
expD12	RCP8.5	IPSL-CM5A-MR	MeanAnt ₅	Off
expD13	SSP5-85	CNRM-CM6-1	MeanAnt ₉₅	Off
expD14	SSP5-85	CNRM-CM6-1	MeanAnt ₅	Off
expD15	SSP5-85	UKESM1-0-LL	MeanAnt ₉₅	Off
expD16	SSP5-85	UKESM1-0-LL	MeanAnt ₅	Off
expD17	SSP5-85	CESM2	MeanAnt ₉₅	Off
expD18	SSP5-85	CESM2	MeanAnt ₅	Off
expD51	RCP8.5	NorESM1-M	PIG ₅	Off
expD52	RCP8.5	NorESM1-M	PIG ₉₅	Off
expD53	RCP8.5	MIROC-ESM-CHEM	PIG ₅₀	Off
expD54	RCP8.5	MIROC-ESM-CHEM	PIG ₅	Off
expD55	RCP8.5	MIROC-ESM-CHEM	PIG ₉₅	Off
expD56	RCP8.5	CCSM4	PIG ₅₀	Off
expD57	RCP8.5	CCSM4	PIG ₅	Off
expD58	RCP8.5	CCSM4	PIG ₉₅	Off
expT071	RCP2.6	NorESM1-M	PIG ₅₀	Off
expT072	RCP2.6	NorESM1-M	PIG ₅	Off
expT073	RCP2.6	NorESM1-M	PIG ₉₅	Off
Ice shelf collapse under different climate forcings				
expE6	RCP8.5	NorESM1-M	MeanAnt ₅₀	On
expE7	RCP8.5	MIROC-ESM-CHEM	MeanAnt ₅₀	On
expE8	RCP8.5	HadGEM2-ES	MeanAnt ₅₀	On
expE9	RCP8.5	CSIRO-Mk3-6-0	MeanAnt ₅₀	On
expE10	RCP8.5	IPSL-CM5A-MR	MeanAnt ₅₀	On
Ice shelf collapse and basal melt interactions				
expTD5	RCP8.5	CCSM4	MeanAnt ₉₅	On
expTD56	RCP8.5	CCSM4	PIG ₅₀	On
expTD58	RCP8.5	CCSM4	PIG ₉₅	On

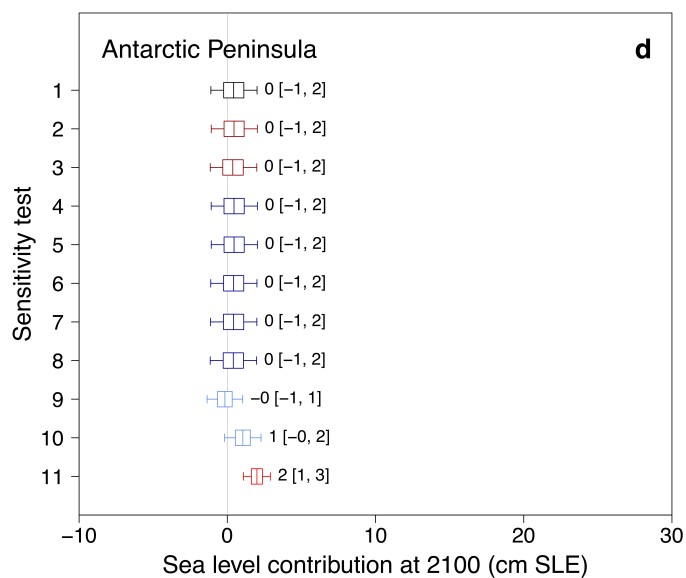
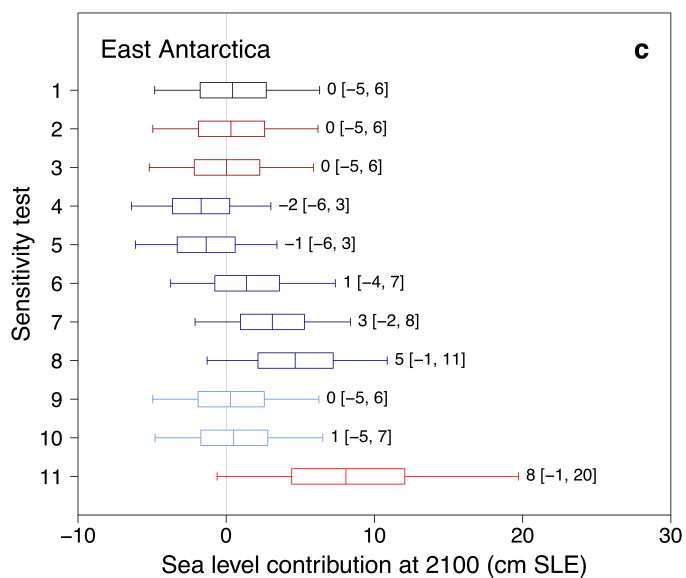
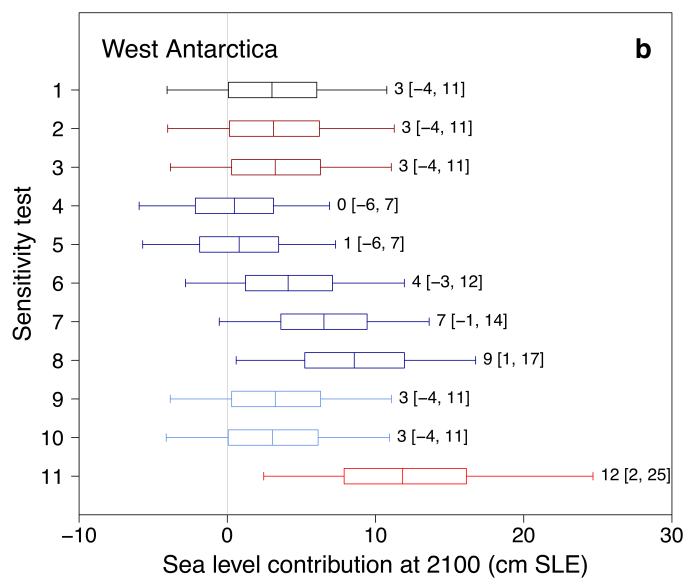
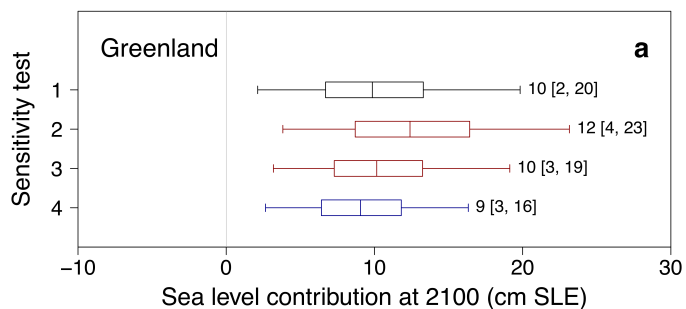
Region	Covariance function and hyperparameters (α : exponent; ν : roughness parameter)	% predictions within emulator 95% interval	Mean absolute error (cm)
Greenland ice sheet	power exp ($\alpha = 0.1$)	94.1	1.4
West Antarctica	power exp ($\alpha = 0.1$)	93.6	2.0
East Antarctica	power exp ($\alpha = 0.1$)	94.8	1.5
Antarctic Peninsula	power exp ($\alpha = 0.1$)	92.4	0.28
1: Alaska	power exp ($\alpha = 1.0$)	95.5	0.55
2: Western Canada and U.S.	power exp ($\alpha = 1.9$)	96.1	0.040
3: Arctic Canada North	power exp ($\alpha = 1.9$)	92.7	0.51
4: Arctic Canada South	power exp ($\alpha = 0.1$)	95.5	0.27
5: Greenland periphery	power exp ($\alpha = 0.1$)	94.9	0.36
6: Iceland	power exp ($\alpha = 1.0$)	95.5	0.13
7: Svalbard	power exp ($\alpha = 0.1$)	95.5	0.37
8: Scandinavia	power exp ($\alpha = 1.0$)	98.3	0.012
9: Russian Arctic	power exp ($\alpha = 1.0$)	94.9	0.41
10: North Asia	power exp ($\alpha = 1.0$)	89.3	0.0084
11: Central Europe	power exp ($\alpha = 1.0$)	97.4	0.0044
12: Caucasus	Matérn ($\nu = 3/2$)	96.6	0.0020
13: Central Asia	power exp ($\alpha = 0.1$)	95.1	0.15
14: South Asia (West)	power exp ($\alpha = 1.9$)	96.4	0.11
15: South Asia (East)	power exp ($\alpha = 0.1$)	91.5	0.045
16: Low Latitudes	power exp ($\alpha = 0.1$)	95.5	0.0054
17: Southern Andes	Matérn ($\nu = 5/2$)	92.1	0.16
18: New Zealand	power exp ($\alpha = 0.1$)	94.1	0.0024
19: Antarctic and Subantarctic periphery	Matérn ($\nu = 5/2$)	92.9	0.87







Sensitivity tests	
Description	Impact
2: CMIP6 temperature projections	
Around 30 CMIP6 models are available at the time of analysis for four SSPs (31 for SSP1-26, 30 for SSP2-45, 27 for SSP3-70 and 31 for SSP5-85). Simulations are obtained and processed in the same way as the subset used for the emulator calibration. We set missing 2100 values to that of 2099 (for CAMS-CSM1-0, and two additional models for SSP3-70). We smooth the temperature changes with a kernel density estimator and sample from this with replacement (N = 1000; Extended Data Figure 3).	We find a slight increase in projected sea level rise: median and 95 th percentile land ice contributions increase by 1-5 cm and 4-7 cm across scenarios SSP1-26 to SSP5-85. This is likely due to the greater number of simulations with high equilibrium climate sensitivity in CMIP6 than FaIR (and a wider range than several recent past generations, 1.8-5.6°C) ³⁴ . The FaIR ensemble is constructed to have a climate sensitivity distribution in line with latest understanding from multiple lines of evidence (5-95% range 2-5°C) ³⁰ .
3, 4: Fixed global mean temperature and ice sheet melt parameters	
We replace the input distributions with single values, to test the potential for reducing uncertainties with improved knowledge	Using the FaIR ensemble mean for global temperature, the width of the 5-95% range for SSP5-85 reduces from 30 cm to 26 cm. Using default values of the Greenland retreat and Antarctic basal melt parameters ($\kappa = \kappa_{50}$; $\gamma_0 = \text{MeanAnt}_{50}$), the 5-95% range decreases from 30 cm to 25 cm.
5, 6: Antarctic basal melt - Mean Antarctic and Pine Island Glacier distributions	
We use the Mean Antarctic (test 5), or Pine Island Glacier (test 6) distribution for basal melt γ , rather than the combined distribution, sampling from the original distributions with replacement.	Results are discussed in the main text.
7, 8: Antarctic basal melt - uniform distributions	
We use two uniform distributions to reproduce the sampling strategy of ref [26]. This is an emulation-type study based on a similar ensemble of climate and Antarctic ice sheet models to ISMIP6, which uses a uniform distribution for basal melt sensitivity consistent with values estimated for the Amundsen Sea region ³⁹ . If we add projections of dynamic change from ref. [26] to IPCC AR5 ²⁵ projections for surface mass balance (SMB), neglecting differences in time period, the median projections are ~11 and ~13 cm under RCP2.6 and RCP8.5, and the 95 th percentiles are ~35 and ~54 cm (using median SMB values in both).	We reach similar values only with extreme values of the basal melt parameter: we show here $\gamma \sim \text{unif}[\text{PIG}_{50}, \text{PIG}_{95}]$ and $\gamma \sim \text{unif}[\text{PIG}_{50}, 700000]$, where 700000 is 98.7th percentile of the Pine Island Glacier distribution, which give median projections of 10 cm and ~14 cm across all scenarios. The 95 th percentiles are roughly half those of the other study: ~19 cm and ~24 cm.
9, 10: Antarctic ice shelf collapse off and on	
We use only $C = 0$ or $C = 1$, rather than a random sample of the two.	Results are discussed in the main text.
11: Risk-averse Antarctic projections	
We use the five global climate models with highest sea level contribution or for which ice shelf collapse projections are available (Robustness test 7), the four Antarctic ice sheet models with highest sensitivity to basal melting (Robustness test 6), the Pine Island Glacier distribution for basal melt γ (Sensitivity test 6) and ice shelf collapse on (Sensitivity test 10). We also use the same γ value for all three regions in a given projection, i.e. fully correlated rather than sampled independently, to explore the tails more fully: this aspect broadens the distribution, increasing the 95 th percentile by 2-4 cm and decreasing the 5 th by 1 cm, and also decreases the median by 1 cm. We use N = 5000 temperature samples, as for the main projections. We do not use the combinations that lead to the highest possible sea level contribution – i.e. the single most sensitive ice sheet model (Robustness test 4), or the extreme distributions for basal melt (Sensitivity test 7-8) – because we aim to provide plausible high-end projections, rather than relying on a single model or unrealistic assumptions.	Results are discussed in the main text.



Robustness checks		
Description		Impact
2: High resolution models		
We use only Greenland ice sheet models with minimum spatial resolution less than 8 km (N = 215) and Antarctic ice sheet models with resolution less than 32 km (N = 303).		This results in differences of 0-1 cm for each ice sheet.
3: More balanced design		
We restrict the input dataset to only the models with the most complete designs (i.e. the most experiments). For Greenland, we use 10 of the 21 models: one with 28 experiments (IMAU/IMAUICE1) and the nine models that ran all 14 experiments presented by refs. [14] and [16] (AWI/ISSM1, ISSM2 and ISSM3, ILTS_PIK/SICOPOLIS1 and SICOPOLIS2, JPL/ISSM, LSCE/GRISLI2, NCAR/CISM, VUB/GISMHOMv1), removing the dummy variable from the emulator as there are no 'open' models in this set (N = 154). For Antarctica, we use four of the 16 models (ILTS_PIK/SICOPOLIS: N = 55, of which 13 do not use the ISMIP6 parameterisation; JPL1/ISSM: N = 48; LSCE/GRISLI: N = 47; NCAR/CISM: N = 27) (total N = 177).		This results in differences of 0-1 cm for each ice sheet.
4, 5: Single ice sheet models		
We use only the Greenland model with the most simulations (IMAU/IMAUICE1: N = 28), and a single model for Antarctica (test 4: ILTS_PIK/SICOPOLIS, N = 48; test 5: LSCE/GRISLI, N = 47). The two Antarctic models have high and low sensitivity to the basal melting parameter, respectively (Extended Data Figure 6).		Using one Greenland model has little impact: the largest change is 2 cm increase in the 95 th percentile, due to this model being at the upper end of the range in sensitivity to the retreat parameter (Figure 2a: triangles). Using one Antarctic model has far more effect: results are discussed further in the main text.
6: Highest sensitivity Antarctic ice sheet models		
We use the four Antarctic models with highest sensitivity to basal melting, i.e. largest 2100 contribution for γ = PIG ₅₀ , ice shelf collapse off and RCP8.5/SSP5-85 (decreasing order: ILTS_PIK/SICOPOLIS: N = 48; ULB/ETISh_16km: N = 21; ULB/ETISh_32km: N = 21; DOE/MALI: N = 8) (total N = 98).		Results are discussed in the main text.
7: Select climate models that result in highest Antarctic sea level contributions		
We use only results from the climate models that lead to highest sea level contributions at 2100 under γ = MeanAnt ₅₀ , ice shelf collapse off and RCP8.5/SSP5-85 (in decreasing order: HadGEM2-ES, UKESM1-0-LL, MIROC-ESM-CHEM, NorESM1-M). We also include CCSM4, to retain information on the effect of ice shelf collapse (N = 241). We also test the impact of using only two of these climate models (not shown in Extended Data Figure 5): NorESM1-M (discussed in the main text regarding scenario-dependence: Figure 4) and CCSM4 (for shelf collapse) (N = 164).		Using these five climate models results in +1 cm change to median from SSP1-19 to SSP5-85 for West Antarctica, -1 cm for East Antarctica, and +1 cm for the total. NDCs median increases by +2 cm relative to main projections. Using only NorESM1-M and CCSM4 leads to +2 cm from SSP1-19 to SSP5-85 for West Antarctica, -3 cm for East Antarctica, and -3 cm decrease for the total, i.e. a weak scenario dependence; no change to NDCs median.
8: Exclude Antarctic ice sheet models far from observed trend		
We exclude simulations with 2015-2020 sea level contributions outside the range 0.00-0.60 cm, motivated by recent observations. We use a satellite estimate ⁶⁶ of the mass trend from 2012-2017 (-219 ± 43 Gt a ⁻¹) and reject simulations for which the mean trend over 2015-2020 is outside the mean ± 5 s.d. interval (N = 181). We choose this interval to allow for the trend changing from one time period to the other, and for tolerance to model discrepancy ²⁴ , and because it coincides with zero at the bottom end so is informative for excluding models with mass gain at the start of the projections (as well as those with very rapid mass loss).		This results in +1 cm scenario-dependence for West Antarctica and -2 cm for East Antarctica, and none for the total; the NDCs median increases by 1 cm.
9: Exclude Antarctic ice sheet models that do not use ISMIP6 melt parameterisation		
We exclude the ice sheet models that do not use the ISMIP6 basal melt parameterisation. (N = 282).		No scenario-dependence for West Antarctica or the total; -2 cm for East Antarctica. No change to NDCs median.
10: Impute higher basal melt value for Antarctic ice sheet models that do not use the ISMIP6 melt parameterisation		
We assign models that do not use the ISMIP6 parameterisations a higher value for γ (150,000; slightly less than PIG ₅₀), rather than the ensemble mean (59,317), reflecting the fact that such models are often tuned to Amundsen Sea (high) melt observations, and approximately in line with NCAR/CISM which was run in both modes (Extended Data Figure 6).		This results in +1 cm scenario-dependence for West Antarctica, -1 cm decrease for East Antarctica, and no change for the total; the NDCs median projection decreases by 1 cm.

